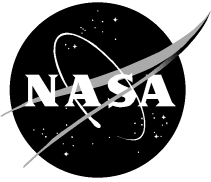# SeaWiFS Postlaunch Technical Report Series

Stanford B. Hooker and Elaine R. Firestone, Editors

Volume 23, Tower-Perturbation Measurements in Above-Water Radiometry

Stanford B. Hooker, Giuseppe Zibordi, Jean-François Berthon, Davide D'Alimonte, Dirk van der Linde, and James W. Brown

The NASA STI Program Office ... in Profile

Since its founding, NASA has been dedicated to the advancement of aeronautics and space science. The NASA Scientific and Technical Information (STI) Program Office plays a key part in helping NASA maintain this important role.

The NASA STI Program Office is operated by Langley Research Center, the lead center for NASA's scientific and technical information. The NASA STI Program Office provides access to the NASA STI Database, the largest collection of aeronautical and space science STI in the world. The Program Office is also NASA's institutional mechanism for disseminating the results of its research and development activities. These results are published by NASA in the NASA STI Report Series, which includes the following report types:

- TECHNICAL PUBLICATION. Reports of completed research or a major significant phase of research that present the results of NASA programs and include extensive data or theoretical analysis. Includes compilations of significant scientific and technical data and information deemed to be of continuing reference value. NASA's counterpart of peer-reviewed formal professional papers but has less stringent limitations on manuscript length and extent of graphic presentations.

- TECHNICAL MEMORANDUM. Scientific and technical findings that are preliminary or of specialized interest, e.g., quick release reports, working papers, and bibliographies that contain minimal annotation. Does not contain extensive analysis.

- CONTRACTOR REPORT. Scientific and technical findings by NASA-sponsored contractors and grantees.

- CONFERENCE PUBLICATION. Collected papers from scientific and technical conferences, symposia, seminars, or other meetings sponsored or cosponsored by NASA.

- SPECIAL PUBLICATION. Scientific, technical, or historical information from NASA programs, projects, and mission, often concerned with subjects having substantial public interest.

- TECHNICAL TRANSLATION. English-language translations of foreign scientific and technical material pertinent to NASA's mission.

Specialized services that complement the STI Program Office's diverse offerings include creating custom thesauri, building customized databases, organizing and publishing research results... even providing videos.

For more information about the NASA STI Program Office, see the following:

- Access the NASA SIT Program Home Page at http://www.sti.nasa.gov/STI-homepage.html

- E-mail your question via the Internet to help@sti.nasa.gov

- Fax your question to the NASA Access Help Desk at (301) 621-0134

- Write to:
  NASA Access Help Desk
  NASA Center for Aerospace Information
  7121 Standard Drive
  Hanover, MD 21076-1320
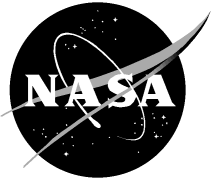
SeaWiFS Postlaunch Technical Report Series

Stanford B. Hooker, Editor
NASA Goddard Space Flight Center, Greenbelt, Maryland

Elaine R. Firestone, Senior Scientific Technical Editor
Science Applications International Corporation, Beltsville, Maryland

Volume 23, Tower-Perturbation Measurements in Above-Water Radiometry

Stanford B. Hooker
NASA Goddard Space Flight Center, Greenbelt, Maryland

Giuseppe Zibordi, Jean-François Berthon, Davide D'Alimonte, and Dirk van der Linde
JRC/Institute for Environment and Sustainability, Ispra, Italy

James W. Brown
RSMAS University of Miami, Miami, Florida

S. Hooker, G. Zibordi, J-F. Berthon, D. D'Alimonte, D. van der Linde, and J. Brown

PREFACE

One of the most perplexing aspects of satellite remote sensing is the efficient and cost effective collection of the high quality field data required for the development of bio-optical and atmospheric correction algorithms and the validation of derived products. With the fourth SeaWiFS reprocessing, approximately 10% of the validation data collected resulted in a match-up comparison after the exclusion criteria were applied. This is a substantial improvement over initial success rates of less than 2% for the radiometric comparisons associated with the first reprocessing. The increased success rates reflect improved data processing procedures and cruise planning based on real-time SeaWiFS data. It is doubtful, however, that significant improvements in present success rates will be possible.

Although sampling from fixed platforms has always been attractive from a cost perspective, light perturbation issues have precluded their extensive use in the past. In addition, unattended subsurface instrumentation, either attached or moored in close proximity to a platform, has problems with biofouling or damage resulting from recreational uses of the platform, e.g., fishing. If a scheme or protocol that minimizes the perturbation effects to acceptable levels can be defined, a substantial reduction in cost per matchup can be realized. This is particularly important for coastal regions where temporal and spatial variability is high, making frequent sampling important, and the accuracy of subsurface measurements is compromised by instrument self-shading and large subsurface vertical gradients.

The work presented in this technical report addresses these issues in an effort to establish a viable above-surface protocol for platforms and shows that such a protocol should be possible. Finally, the study helps support the argument that continued investment in field data collection protocols and technology is very cost effective and needs to be included in future remote sensing programs, especially because the SeaWiFS and SIMBIOS Projects, which have funded much of this research, are coming to an end this year.

Greenbelt, Maryland — C. R. McClain
January 2003

Table of Contents

S. Hooker, G. Zibordi, J-F. Berthon, D. D'Alimonte, D. van der Linde, and J. Brown

Table of Contents (*cont.*)

S. Hooker, G. Zibordi, J-F. Berthon, D. D'Alimonte, D. van der Linde, and J. Brown

Abstract

This report documents the scientific activities which took place during June 2001 and June 2002 on the *Acqua Alta* Oceanographic Tower (AAOT) in the northern Adriatic Sea. The primary objective of these field campaigns was to quantify the effect of platform perturbations (principally reflections of sunlight onto the sea surface) on above-water measurements of water-leaving radiances. The deployment goals documented in this report were to: a) collect an extensive and simultaneous set of above- and in-water optical measurements under predominantly clear-sky conditions; b) establish the vertical properties of the water column using a variety of ancillary measurements, many of which were taken coincidently with the optical measurements; and c) determine the bulk properties of the environment using a diversity of atmospheric, biogeochemical, and meteorological techniques. A preliminary assessment of the data collected during the two field campaigns shows the perturbation in above-water radiometry caused by a large offshore structure is very similar to that caused by a large research vessel.

Prologue

Ocean color satellite sensors (IOCCG 1998) provide large-scale synoptic observations of biogeochemical properties of the upper layer in the open ocean (e.g., phytoplankton biomass), as well as continuous monitoring of other important parameters in the coastal zones (e.g., sediment load and dissolved colored matter). This global capability is accomplished through the determination of radiometric quantities, specifically the spectral values of the radiances at the top of the atmosphere, from which (after atmospheric correction), the radiances emerging from the ocean surface, $L_W(\lambda)$, the so-called *water-leaving radiances*, are extracted (λ denotes the wavelength).

For meaningful applications, an extremely high radiometric accuracy is required. The Sea-viewing Wide Field-of-view Sensor (SeaWiFS) Project, for example, requires accuracies of 5% absolute and 1% relative in terms of the retrieved $L_W(\lambda)$ values (Hooker and Esaias 1993). The first obvious condition for reaching such an accuracy lies in the conception and the realization of the spaceborne instrument. Although this is a necessary requirement, it is not sufficient to ensure the distributed radiometric data meet the accuracy objectives. Indeed, the success of the SeaWiFS mission is determined in particular by the quality of the ocean color data set collected for calibration and validation purposes, and involves several continuous activities (McClain et al. 1992):

1. Characterizing and calibrating the sensor system,

2. Analyzing trends and anomalies in the sensor performance and derived products (the L_W values and the chlorophyll concentration),

3. Supporting the development and validation of algorithms (for the retrieval of bio-optical properties and for atmospheric correction), and

4. Verifying the processing code and selecting ancillary data (e.g., ozone, wind, atmospheric pressure) used in the data processing scheme.

The initial SeaWiFS validation results (Hooker and McClain 2000) provided an immediate and quantitative demonstration of the strengths of the initial calibration and validation plan (McClain et al. 1998): a) the sensor was stable over the first two years of operation, with gradual changes in some wavelengths being accurately quantified using the solar and lunar calibration data; b) the vicarious calibration approach using field data produced consistent $L_W(\lambda)$ values; and c) the remotely-sensed products, including the (total) chlorophyll a concentration, met the desired accuracy (35% over a range 0.05–50 $\mathrm{mg\,m^{-3}}$) over a limited, albeit diverse, set of open-ocean validation sites.

The study presented here does not deal with all aspects of the calibration and validation process. It is restricted to those field measurements suitable for vicarious calibration, as well as the derivation or improvement of bio-optical algorithms. Historically, the fundamental radiometric quantities selected for comparison with the radiances retrieved from the spaceborne sensor, were the upwelled spectral radiances just above the sea surface, $L_W(0^+, \lambda)$ (the symbol 0^+ means immediately above the surface). A variety of normalizations of these radiances are needed to render these quantities less dependent on the circumstances (in particular, on the solar illumination conditions prevailing when the measurements are performed), and thus to obtain more fundamental quantities to be introduced into the bio-optical algorithms.

The $L_W(0^+, \lambda)$ radiances can be derived by extrapolating in-water measurements taken close to the sea surface or obtained directly from above-water measurements. Although the SeaWiFS Project has placed an emphasis on in-water techniques, which have been largely successful in Case-1 waters (Hooker and Maritorena 2000), both measurement approaches have advantages and difficulties. The above-water approach for vicarious calibration remains attractive, because a) the data can presumably be collected

more rapidly and from a ship underway, and b) the frequently turbid and strongly absorbing waters in shallow Case-2 environments impose severe limitations on in-water measurements. The latter includes the difficulty of resolving the thin optically different layers usually encountered in coastal waters, and properly correcting for the instrument self-shading effect.

From a measurement perspective, the above-water approach is more restrictive, because presently there is no reliable mechanism for floating an above-water system away from a measurement platform (which is easily and effectively accomplished for an in-water system), so all above-water measurements are made in close proximity to a large structure.

Measurement and analysis protocols were recommended (Mueller and Austin 1992) and were incrementally revised (Mueller and Austin 1995, Mueller 2000, and Mueller 2002) for both methods, but a methodology for correcting above-water data for platform perturbations does not yet exist. A capability to detect and quantify the reflective perturbation of the sampling platform in above-water data was recently presented by Hooker and Morel (2003), and this technique forms the central analytical approach for the primary objective of the present study: to establish the spatial extent of platform perturbations in above-water data.

The field measurements for determining the effects of a large platform on above-water radiometry were carried out on the *Acqua Alta* Oceanographic Tower (AAOT) in the northern Adriatic Sea (12.508°E,45.314°N) and within the framework of the Coastal Atmosphere and Sea Time Series (CoASTS) Project (Zibordi et al. 2002a) led by Joint Research Centre (JRC) of the Commission of the European Communities in Ispra, Italy. The measurement site is located approximately 15 km offshore the Venice Lagoon in a frontal region that can be characterized by Case-1 or Case-2 conditions.

Regardless of the water type during any given measurement opportunity, the AAOT is a coastal ocean site, so its use for the tower-shading campaigns ensured a large variety of environmental parameters and complexity being represented in the data set. A detailed description of using the AAOT for specialized experiments, the CoASTS sampling objectives, and the environmental features of the site are given in Hooker et al. (1999), Zibordi et al. (2002a), and Berthon et al. (2002), respectively, so only brief overviews are presented here.

An international group of scientists were deployed to the AAOT from 18–29 June 2001 and then again from 17–28 June 2002. The scientists were from, or associated with, the National Aeronautics and Space Administration (NASA) Goddard Space Flight Center (GSFC), and the Institute for Environment Sustainability (IES) Inland and Marine Waters Unit† of the JRC.

---

† Formerly the Space Applications Institute (SAI) Marine Environment Unit.

To satisfy the objective of determining the spatial scale and radiometric characteristics of tower perturbations in above-water measurements, two activities with the requisite expertise were brought together: the NASA contingent participated as part of the fourth and fifth Sea-WiFS Bio-Optical Algorithm Round-Robin field exercises (SeaBOARR-01 and SeaBOARR-02, respectively), and the JRC team participated as part of the regularly scheduled, but temporally extended, CoASTS campaigns. The science team members from these organizations are given in Appendix A.

1.   In Situ Sampling Equipment

The *in situ* sampling equipment used during the tower-perturbation campaigns was a combination of the instruments normally used in the CoASTS Project and those needed for the specialized measurements associated with quantifying the perturbation of the tower in above-water radiance measurements. The former includes a large diversity of marine and atmospheric measurements for the calibration and validation of ocean color remote sensors, while the latter includes a new above-water optical system with a specialized positioning capability. CoASTS field activities have also been used as an opportunity to evaluate new instruments designed for the special circumstances associated with the coastal environment. Within this objective, the tower-perturbation campaigns were used to begin a preliminary evaluation of a new in-water profiler.

2.   The Horizontal Deployment System (HDS)

The HDS was primarily designed to support investigations for determining tower perturbations in above-water radiometric measurements. The system consists of a tubular horizontal mast sliding within rigidly mounted support frames. The mast is 21 m long and is composed of eight aluminum trusses plus a specially designed terminal end for affixing an instrument package. Each support frame encloses the mast with eight rollers with stainless steel bearings and permits the mast to be moved by a single operator. The HDS has the capability of carrying an instrument package weighing approximately 10 kg, and to deploy it up to as much as 12 m away from the main tower superstructure with a vertical deflection of the mast less than 1% (i.e., less than a 10 cm drop in the vertical for a 10 m extension in the horizontal).

3.   In Situ Methods

The *in situ* methods used during the tower-shading campaigns were a direct consequence of making above- and in-water measurements of the radiance field within the coastal ocean environment. The in-water measurements were intended as a *reference* or ground truth, because previous campaigns had established a methodology for correcting the in-water data for tower perturbation effects. Much of the above-water experiments, however, were by definition degraded—they were specifically designed to

S. Hooker, G. Zibordi, J-F. Berthon, D. D'Alimonte, D. van der Linde, and J. Brown

capture the perturbation of the tower in the surface radiance field. The spatial complexity (primarily vertically for the duration of the experiments considered here) of the coastal ocean makes the interpretation of optical profiles alone very difficult, so a variety of supporting measurements and methods were used to produce a thorough description of the vertical properties of the water column.

4. Advances in Data Processing Methods

New versions of the data processing methods were created to accommodate a) the incorporation of an automated system for determining the ratio of diffuse-to-direct solar irradiance, and b) the correction for bidirectional effects in the above-water (sea-viewing) measurements. The former required a more sophisticated correction to the occulted solar reference data, and the latter required a more complete formulation of the above-water method. Neither advancement altered the type of data collected or the basic data collection methodology.

5. Preliminary Results

The analytical results are organized by separating the above-water radiometric data into near- and far-field categories. The former correspond to data for which $x < 13\,\mathrm{m}$, and the latter to data for which $x \geq 13\,\mathrm{m}$, where x is the perpendicular distance of the surface spot viewed by the sea-viewing sensor away from the tower. The far-field observations confirm uncontaminated above-water data can be collected in the vicinity of a large structure as long as the surface spot is as far away from the platform as it is high (in this case about $13\,\mathrm{m}$). The near-field data show significant perturbations, as much as 100% above far-field levels, which are substantially above any fluctuations that could be attributed to natural environmental variability (in the absence of floating material). A separate investigation of both the widespread and the sporadic effects of floating material showed perturbations as much as 25% above normal (uncontaminated) levels.

Chapter 1

In Situ Sampling Equipment

STANFORD B. HOOKER
NASA/Goddard Space Flight Center
Greenbelt, Maryland

GIUSEPPE ZIBORDI
JRC/IES/Inland and Marine Waters Unit
Ispra, Italy

ABSTRACT

The *in situ* sampling equipment used during the tower-perturbation campaigns was a combination of the instruments normally used in the CoASTS Project and those needed for the specialized measurements associated with quantifying the perturbation of the tower in above-water radiance measurements. The former includes a large diversity of marine and atmospheric measurements for the calibration and validation of ocean color remote sensors, while the latter includes a new above-water optical system with a specialized positioning capability. CoASTS field activities have also been used as an opportunity to evaluate new instruments designed for the special circumstances associated with the coastal environment. Within this objective, the tower-perturbation campaigns were used to begin a preliminary evaluation of a new in-water profiler.

1.1 INTRODUCTION

The emphasis for the tower-perturbation experiments was on measuring the apparent optical properties (AOPs) of seawater. To accomplish this, the optical systems deployed at the AAOT were as follows:

1. The JRC version of the miniature NASA Environmental Sampling System (miniNESS),

2. The Wire-Stabilized Profiling Environmental Radiometer (WiSPER),

3. The micro NASA Environmental Sampling System (microNESS),

4. The micro Surface Acquisition System (microSAS), and

5. The SeaWiFS Photometer Revision for Incident Surface Measurements (SeaPRISM).

The first three instruments are in-water profiling systems, and the last two are above-water instruments. The microNESS instrument was included to compare this new profiler with the well-established capabilities of miniNESS and WiSPER in the coastal environment. The SeaPRISM instrument was included, because it was the first operational version of this new measurement system. Detailed descriptions of each measurement system are presented in Sect. 1.3.

In addition to the AOP measurements, a variety of other data, primarily associated with measuring the inherent optical properties (IOPs) of seawater, were collected to characterize the optical properties of the site in more detail:

6. Attenuation and absorption profiles at nine wavelengths by AC-9† measurements; and

7. *In vivo* spectral absorption of particulate matter and the concentration of colored dissolved organic matter (CDOM) through spectrophotometric techniques.

To ensure the AOP and IOP data can be understood in terms of the large-scale environmental properties, the following biological, hydrographic, and atmospheric data were collected:

8. Pigment concentration using the high performance liquid chromatography (HPLC) technique;

9. The concentration of total suspended matter (TSM) through gravimetric filter analysis;

10. Direct sun irradiance and sky radiance sequences by sun photometer measurements;

---

† Identification of commercial products to adequately specify or document the experimental problem does not imply recommendation or endorsement, nor does it imply that the equipment is necessarily the best available for the purpose.

11. Atmospheric pressure, humidity, and temperature, plus wind speed and direction; and

12. Seawater temperature and salinity with a conductivity, temperature, and depth (CTD) sensor, plus tide level.

It is important to remember the IOP and CTD profiles can be used as an aid to properly interpret and analyze the AOP radiometric profiles. Indeed, in the coastal environment, the presence of thin layers of differing water or optical types makes this a necessity.

1.2 THE AAOT

The water depth immediately below the tower is about 17 m, and the composition of the nearby sea floor is primarily sand and silt. The tower was built in 1970 and is owned and operated by the *Istituto per lo Studio della Dinamica delle Grandi Masse* (ISDGM) of the Italian *Consiglio Nazionale delle Ricerche*† (CNR), in Venice.

In addition to an access platform at the sea surface, the tower is composed of four levels supported by four large pillars. Each level is approximately $7.2\,\text{m}\times5.2\,\text{m}$ in size with the exception of the lowest level which is $5.2\,\text{m}\times5.2\,\text{m}$. The primary reason for selecting the AAOT for the tower-perturbation experiments was the need for a very stable platform to accommodate a positioning system for an above-water sensor system that would allow the horizontal distance between the sensors and the tower to be varied (the HDS is described in Chapt. 2).

The first (lowest) tower level, about 4.5 m above the water, has an open grid deck and no facilities. The second level is approximately 7 m above the water and contains a workshop with dual electrical generators, a portable laboratory for water filtration and data acquisition, plus storage spaces for a large complement of lead-acid batteries, fuel tanks, etc. The second level also contains a special open grid platform, 3.5 m wide, which extends 6.5 m over the sea towards the southeast. The platform provides mounting points for instruments to be deployed above, or into, the sea, and is the permanent deployment site for the WiSPER instrument frame (it is also the usual launching and recovering site for free-fall profilers).

The third deck contains the main laboratory, which is also used for overnight accommodations. The fourth (highest) deck, at about 13 m above the water, contains solar panels, a variety of meteorological instruments, communications antennae, and water storage tanks. For the tower-perturbation campaigns, the HDS was mounted on the fourth level, so an above-water instrument system (micro-SAS) could be positioned at varying distances with respect to the side of the platform. The SeaPRISM instrument and a CE-318 sun photometer were also mounted on this level. A schematic of the AAOT with the deployment locations

† The Institute for the Study of Large Masses of the Italian National Research Council.

for the optical sensors is shown in Fig. 1, and Fig. 2 shows the AAOT with the HDS extended 10 m over the water.
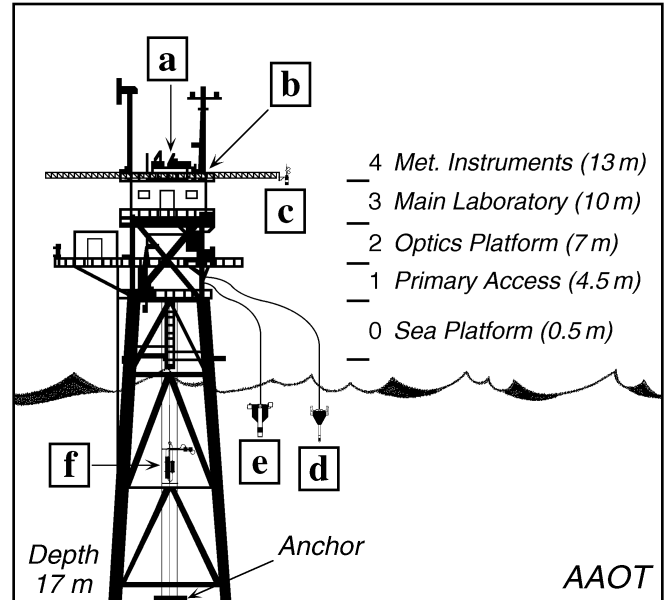
Fig. 1. A schematic of the northwest side of the tower-perturbation deployment locations for **a)** the CE-318 sun photometer, **b)** SeaPRISM, **c)** micro-SAS at the end of the HDS, **d)** microNESS, **e)** mini-NESS, and **f)** WiSPER.

1.3 AOP INSTRUMENTS

The AOP instruments used in the tower-perturbation campaigns were deployed to provide vertical profiles of the *in situ* light field within the water column (WiSPER and miniNESS) and at variable distances away from the AAOT (miniNESS only).

1.3.1 In-Water Instruments

The SeaWiFS Field Team has been working with Satlantic, Inc. (Halifax, Canada), to develop a series of free-falling, modular profilers to measure the optical properties of seawater. The first of these was the Low-Cost NASA Environmental Sampling System (LoCNESS), so called because it was built out of the (relatively inexpensive) modular components typically used with traditional winch and crane deployment systems: the Ocean Color Radiance and Irradiance series 200 (OCR-200 and OCI-200, respectively) seven-channel (λ_7) light sensors, plus a conductivity and temperature probe, and a miniature fluorometer (Aiken et al. 1998).

The LoCNESS profiler was an extremely capable unit (Hooker and Maritorena 2000), which included a three-sensor version permitting the measurement of upwelled radiance, plus upward and downward irradiance as a function of depth z, $L_u(z,\lambda)$, $E_u(z,\lambda)$, and $E_d(z,\lambda)$, respectively. It was difficult to use in small boat operations or in the shallow water normally associated with coastal (nominally

Fig. 2. The AAOT showing the different levels (along with their heights above the water), one of the small boats used to transport people and equipment to the tower, and the HDS on the very top. The inset circular panel shows a closeup of the microSAS instruments mounted at the end of the latter.

Case-2) conditions, however; the overall length was 1.8 m, the diameter of the individual system components was approximately 9 cm, the weight in air was 23 kg, and the light sensors were not mounted on the same horizontal plane—they were separated by the length of the profiler.

1.3.1.1 miniNESS

A smaller version of LoCNESS, called miniNESS, was built to determine whether or not light sensors could be mounted on the fins (in the same horizontal plane) in a more compact configuration without degrading the light field measurements. Intercomparisons of miniNESS with traditional profilers established the efficacy of the new concept during open ocean cruises, and then subsequently during coastal campaigns on the AAOT. In fact, the design was so successful, the JRC combined the modular, three-sensor configuration of the LoCNESS instrument with the original miniNESS design to produce a very unique instrument for coastal ocean applications that measured $L_u(z, \lambda)$, $E_u(z, \lambda)$, and $E_d(z, \lambda)$. This more capable version of miniNESS is part of the routine data collection during CoASTS field campaigns and is the one discussed in this study.

A schematic of the JRC miniNESS profiler is shown in Fig. 3. In addition to the profiler radiometers, a separate sensor measured the total solar irradiance (the direct plus the indirect or diffuse components) just above the sea surface, $E_d(0^+, \lambda)$. During the campaign in 2001, an occulter or *lollipop* was periodically used at the conclusion of some casts to block the direct solar irradiance, so the indirect (or diffuse) component, $E_i(0^+, \lambda)$, could be measured. For the most recent campaign in 2002, a modified version of a shadow band attachment system called Sea-SHADE (Hooker and Lazin 2000) was added to remotely collect the diffuse irradiance data by toggling a switch to activate a shadow band.
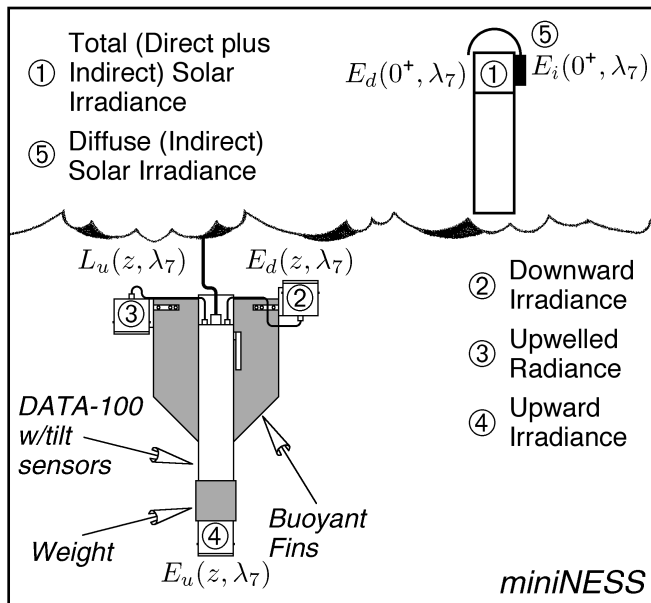
Fig. 3. A schematic of the JRC miniNESS profiler.

1.3.1.2 WiSPER

The WiSPER system also measured $L_u(z, \lambda)$, $E_u(z, \lambda)$, and $E_d(z, \lambda)$. Unlike miniNESS, which had internal tilt sensors to quantify the vertical (two-axis) tilt (φ) of the profiler as it fell through the water, WiSPER was slowly winched up and down the water column between two taught wires fixed between the tower and the sea bottom, so it had no need for tilt sensors. The light sensors were mounted on an extension boom, which placed them 1 m away from the main part of the frame and approximately 7.5 m from the tower legs. The solar reference for WiSPER was the same one used for miniNESS. A schematic of the WiSPER system is shown in Fig. 4.
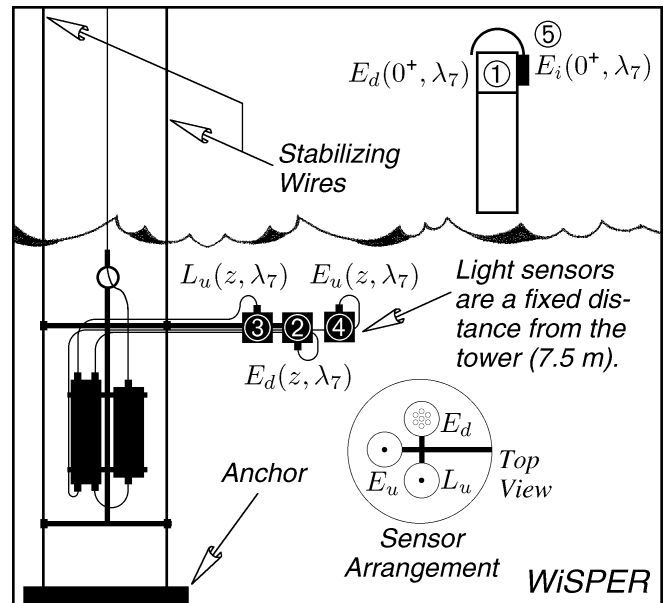
Fig. 4. A schematic of the JRC WiSPER system.

1.3.1.3 microNESS

The success of miniNESS led to a new design effort to further decrease the overall size and weight of the profiling package. At the same time, there was a strong desire to replace the analog cabling associated with traditional profilers with digital interfaces. The latter was particularly important, because when it was combined with the desired size reduction, it would help ensure, with respect to the original equipment:

1. A lowering of power requirements,

2. Smaller, lighter profiler with a lower descent speed and, thus, a higher vertical sampling resolution,

3. A reduction in the perturbation caused by the instrument to the *in situ* light field, and

4. A profiling system that could easily be deployed from a small boat.

The latter three are especially important for coastal (nominally Case-2) applications, because the vertical structure

of the water column is frequently more complex, the water is more turbid (so instrument self-shading is a bigger problem), and shallow areas are only accessible with small boats.

The digital light sensors are called the OCR-507-R series, and the new instrument is called microNESS. Together, they have the following characteristics: a) operation from two 9 V lithium batteries, b) high-accuracy pressure sensing (0.01% full-scale accuracy versus 0.25% for standard Satlantic profilers), c) component diameters of 4.6 cm or less (3.8 cm for the main pressure housing), d) a digital instrumentation network (supporting multiple sensors), e) data sampling of 6 Hz, f) 24-bit resolution of the optical data, g) an overall length of 1.0 m, and h) an in-air weight of 4 kg (miniNESS and LoCNESS have an in-air weight of 15 and 23 kg, respectively). The prototype microNESS profiler was evaluated in the field during simultaneous deployments of the miniNESS profiler in deep ocean (Case-1) conditions.

The microNESS profiler measured $L_u(z, \lambda)$ and $E_d(z, \lambda)$ using two sets of 4-channel (λ_4) optical sensors—the 412 nm channel was common to both sensor sets to enable a simple test for shading effects. The solar reference for microNESS, $E_d(0^+, \lambda)$, had only seven channels and was designed to fit inside a cardanic gimbal (not used for the tower campaigns). The microNESS profiler (Fig. 5) has a similar overall length with respect to the original miniNESS design, but is considerably lighter and capable of a lower descent rate (approximately $0.3\,\mathrm{m\,s^{-1}}$ versus about 0.6–$1.0\,\mathrm{m\,s^{-1}}$ for miniNESS in untethered deployments) and, thus, a higher vertical sampling resolution.
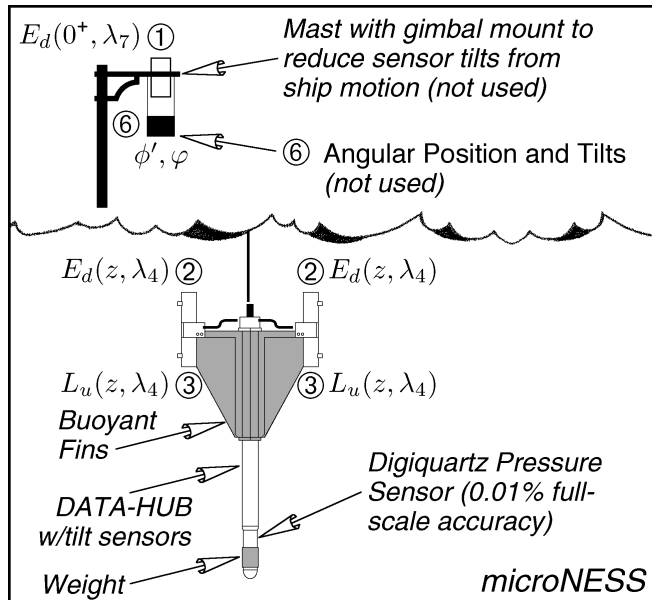
Fig. 5. A schematic of the microNESS profiler. The gimbal ballast contains sensors to determine the azimuthal orientation of the irradiance sensor, ϕ', as well as its two-axis vertical tilt, φ. Neither sensor was used for the tower-perturbation analyses, and are shown simply for completeness.

1.3.2 Above-Water Instruments

The above-water instruments were designed to derive the water-leaving radiance in the same blue-green bands as the in-water systems.

1.3.2.1 microSAS

The microSAS instruments measured the sky radiance reaching the sea surface, $L_i(0^+, \lambda)$, and the (total) radiance right above the sea surface, $L_T(0^+, \lambda)$. Although microNESS and microSAS had separate solar references, only one was used at a time (the output of the irradiance sensor was sent to both data acquisition systems). The reference gimbal was not used during the tower campaigns.

The microSAS deployment frame was based on the Sea-WiFS Underway Surface Acquisition System (SUnSAS) design (Hooker and Lazin 2000). The primary differences are a result of trying to make the entire system as small as possible, so it can be fitted inside a cardanic gimbal. The mechanical frame is a compact mounting system wherein the light sensors are clamped to two small plates, which can be tilted to the desired nadir and zenith angles (nominally 30–45°). The mounting plates are mechanically secured at the desired angles using aluminum wedges cut at the appropriate angles (which permits accurate repeatability). A schematic of microSAS mounted on the terminal end of the HDS mast is presented in Fig. 6, and a closeup picture of the system is shown in Fig. 1 (inset circle).
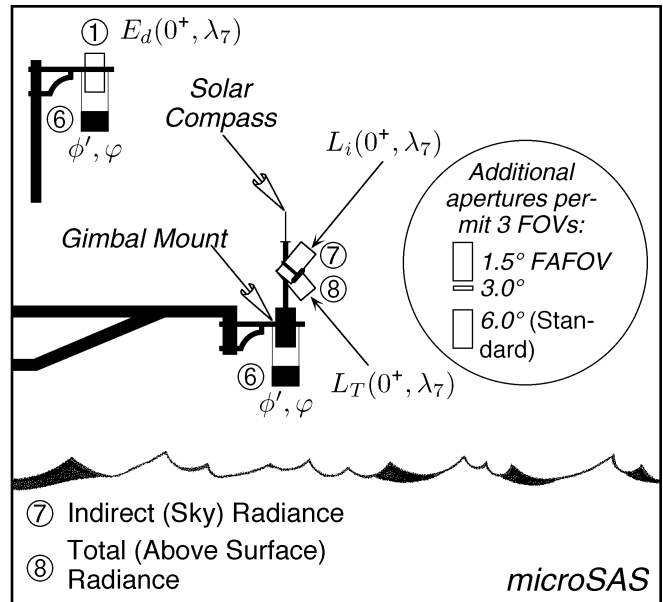
Fig. 6. A schematic of the microSAS instruments. The inset circle shows the new full-angle field of view (FAFOV) as apertures are added to the standard configuration.

The radiance sensors can be rotated 360° in the azimuthal plane, and a band, marked in 10° increments with a 1° vernier, allows for a precise positioning of the frame

with respect to the sun. A *solar compass* or sun dial at the top of the instrument allows for rapid pointing of the entire package with respect to the sun plane. The restoring mass for the gimbal has built-in sensors to measure the compass heading of the system as well as the vertical (two-axis) tilt. The tilt sensors were used to ensure the sensors were level before any data acquisition was initiated.

One of the unique aspects of the microSAS light sensors is the FAFOV can be decreased by adding one or more additional apertures to the basic instrument (which has a 6.0° FAFOV). Addition of the first aperture produces a 3.0° FAFOV, and adding the second produces a 1.5° FAFOV. The latter is more similar to the 1.2° SeaPRISM FAFOV. Although data for all three aperture settings were collected, the majority of the data was for a 6.0° FAFOV.

All of the sensors were powered with a 12 V battery, and they took and reported data simultaneously (via RS-485 serial communications). The data were logged on a Macintosh PowerBook computer using software developed at the University of Miami Rosenstiel School for Marine and Atmospheric Science (RSMAS) and the SeaWiFS Project. The sensor data were time stamped and recorded to disk as American Standard Code for Information Interchange (ASCII), tab-delimited (spreadsheet) files. The operator controlled the logging and display of the data as a function of the acquisition activity: dark data (caps on the radiometers), sea and sky viewing, etc. The initiation of the execution mode automatically set the file name and file headers, as well as the timed termination of the data acquisition. All of the telemetry channels were displayed and visualized in real time.

1.3.2.2 SeaPRISM

SeaPRISM is based on a CE-318 sun photometer (Sect. 1.6.1) made by CIMEL Electronique (Paris, France). The CE-318 is an automated system which measures the direct sun irradiance, $E(\lambda)$ at solar zenith angle θ and solar azimuth angle ϕ, plus the sky radiance in the sun and almucantar planes. The data are transmitted over a satellite link, and this remote operation capability has made the device very useful for atmospheric measurements. The revision to the CE-318 that makes the instrument useful for ocean color calibration and validation activities is to include a capability for measuring the sea and sky radiances at the appropriate vertical angles (ϑ and ϑ', respectively) in wavelengths suitable for the determination of chlorophyll a concentration.

The initial evaluation of the SeaPRISM prototype involved above- and in-water measurement protocols (Hooker et al. 2000a). A long-term intercomparison (lasting approximately one year) of the water-leaving radiances derived from SeaPRISM and the WiSPER in-water system (Zibordi et al. 2002b) showed the overall spectral agreement was approximately 8.6%, but the blue-green channels intercompared at the 5% level; a blue-green band ratio comparison was at the 4% level. A schematic of the SeaPRISM instrument is shown in Fig. 7.
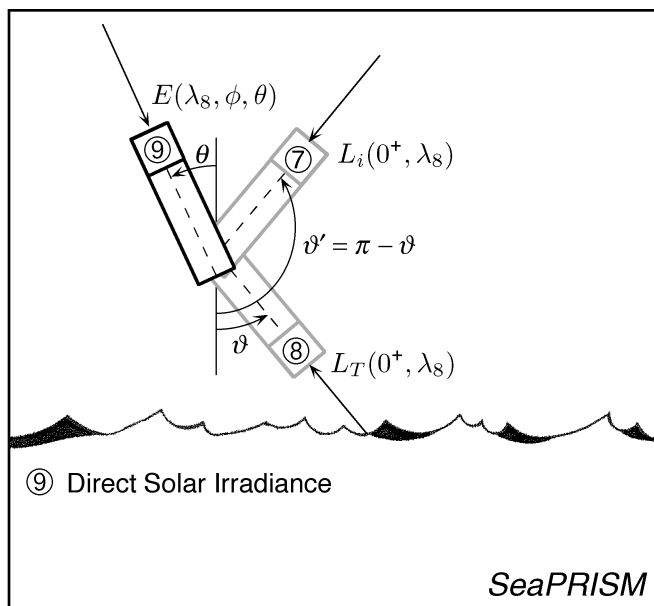
Fig. 7. A schematic of the SeaPRISM instrument.

1.3.3 Summary

A summary of the AOP instruments, along with their primary physical measurements, and their sensor codes are given in Table 1; Table 2 presents the sensor wavelengths.

Table 1. A summary of the radiometers used during the tower perturbation field campaigns along with their primary physical measurement (in terms of their vertical sampling), their spectral resolution (λ_i means i channels, i.e., λ_7 means 7 channels), and their sensor codes. The M099 sensor was periodically occulted to measure $E_i(0^+, \lambda_7)$.

System	Sensor	Measurement	Code
miniNESS	OCR-200	$L_u(z, \lambda_7)$	R067
	OCI-200	$E_d(z, \lambda_7)$	I097
	OCI-200	$E_u(z, \lambda_7)$	I098
	OCI-200	$E_d(0^+, \lambda_7)$	M099
WiSPER	OCR-200	$L_u(z, \lambda_7)$	R046
	OCI-200	$E_d(z, \lambda_7)$	I071
	OCI-200	$E_u(z, \lambda_7)$	I109
	OCI-200	$E_d(0^+, \lambda_7)$	M099
microNESS	OCR-504-R	$L_u(z, \lambda_4)$	S001
	OCR-504-R	$L_u(z, \lambda_4)$	S002
	OCR-504-I	$E_d(z, \lambda_4)$	K001
	OCR-504-I	$E_d(z, \lambda_4)$	K002
	OCR-507-I	$E_d(0^+, \lambda_7)$	O001
microSAS	OCR-507-R	$L_i(0^+, \lambda_7)$	U010
	OCR-507-R	$L_T(0^+, \lambda_7)$	U003
	OCR-507-I	$E_d(0^+, \lambda_7)$	O026
SeaPRISM	CE-318	$E(0^+, \lambda_8)$	C318
	CE-318	$L_i(0^+, \lambda_8)$	C318
	CE-318	$L_T(0^+, \lambda_8)$	C318

Table 2. Individual channel numbers, λ_i, and center wavelengths (in nanometers) for the radiometers used with the radiometric sampling systems (10 nm bandwidths). The sensors for each system are given with their individual sensor codes, which are formed from a three-digit model or serial number (S/N), preceded by a one-letter designator for the type of sensor: R and S, in-water radiance; I and K, in-water irradiance; M and O, above-water irradiance; and U or C, above-water radiance. The M099 WiSPER reference was used with miniNESS and WiSPER. For microNESS, the "K001,2" and "S001,2" entries mean the four channels for K001 and S001 are given as channels 1–4, and the four channels for K002 and S002 are given as channels 5–8.

λ_i	WiSPER				miniNESS			microNESS			microSAS			SeaPRISM
	R046	I071	I109	M099	R067	I097	I098	K001,2	S001,2	O001	U003	U010	O026	C318
1	412.3	412.4	412.5	411.5	412.5	412.3	412.4	412.2	412.4	412.2	412.0	412.2	412.2	412
2	442.8	443.5	442.2	442.8	442.2	442.1	443.5	490.9	490.0	443.8	443.1	442.8	442.9	440
3	490.5	490.6	490.7	489.9	490.0	490.5	490.8	509.4	509.2	490.7	490.5	490.9	490.8	501
4	510.8	509.1	509.8	510.3	510.3	510.3	509.9	554.6	554.0	509.3	510.8	510.5	510.0	555
5	554.9	555.9	554.7	554.5	554.5	554.5	554.7	412.4	412.3	554.5	555.1	554.7	554.7	668
6	665.8	665.4	664.8	664.8	665.4	665.7	664.9	442.9	443.0	560.1	559.5	559.1	560.2	870
7	683.9	682.1	683.2	683.2	684.0	683.8	683.2	560.1	560.0	865.1	864.5	864.6	865.1	936
8								865.2	865.5					1018

1.4 IOP INSTRUMENTS

Within the CoASTS measurement campaigns, IOP profiles were simultaneously taken for the beam attenuation $c(z,\lambda)$, absorption $a(z,\lambda)$, and backscattering $b_b(z,\lambda)$ coefficients. The IOP instruments were deployed on the WiSPER frame and lowered at a speed of $0.1 \, \mathrm{m\,s^{-1}}$. In addition to IOP profiles, water samples were collected at discrete depths z_d for additional laboratory analyses. Specifically, spectrometric analysis was made on particulate matter to determine the absorption coefficients of pigmented $a_{ph}(z_d,\lambda)$ and nonpigmented $a_{dp}(z_d,\lambda)$ particles, and on $0.22 \, \mathrm{\mu m}$ filtered seawater to determine the absorption coefficient $a_{ys}(z_d,\lambda)$ of CDOM.

1.4.1 AC-9

The profiles of $c(z,\lambda)$ and $a(z,\lambda)$ were obtained from measurements taken at 412, 440, 488, 510, 555, 630, 650, 676, and 715 nm with a 25 cm path length AC-9 manufactured by Western Environmental Technology Laboratories (WETLabs), Inc. (Philomath, Oregon). The instrument is a system composed of two flow tubes (a beam reflective tube for absorption measurements and a nonreflective tube for beam attenuation measurements) located between the light source unit (including a lamp and a filter wheel with nine spectral filters) plus a detector and acquisition unit (composed of a beam diffuser-receiver for absorption measurements and a beam collimated-receiver for beam attenuation measurements).

A Sea-Bird Electronics (Bellevue, Washington) 5T submersible pump provides a constant flow of water within the tubes. The AC-9 data logging was made using the WETView software (version 5.0A) provided by WETLabs. The AC-9 absolute calibration was carried out on site at the beginning of each measurement campaign using Milli-Q† water, in agreement with the recommended practice (WETLabs 2002).

1.4.2 HYDROSCAT-6

Profiles of $b_b(z,\lambda)$ were obtained at 442, 488, 510, 555, 620, and 670 nm with a HYDROSCAT-6 manufactured by Hydro-Optics, Biology, and Instrumentation (HOBI) Laboratories, Inc. (Tucson, Arizona). The instrument integrates six modulated light sources coupled to detectors measuring the backscattered light of the source at an angle of 140°. The different modulation of the light sources ensures that the receivers only detect the backscattered light at the specific related wavelength.

The HYDROSCAT-6 data were logged and processed using the HydroScat software (version 1.0) provided by HOBI Laboratories. The HYDROSCAT-6 calibration was checked twice a year by the JRC following the procedures recommended by HOBI Labs. (Maffione and Dana 1997).

1.4.3 Lambda-19 and Lambda-12

The determination of the spectral absorption coefficients $a_{ph}(z_d,\lambda)$, $a_{dp}(z_d,\lambda)$, and $a_{ys}(z_d,\lambda)$ for water samples taken at discrete depths, was made using Perkin Elmer Lambda-19 and Lambda-12 dual beam spectrometers. The Lambda-19, which is used to determine both $a_{ph}(z_d,\lambda)$ and $a_{dp}(z_d,\lambda)$, is equipped with a 60 mm diameter barium sulfate integrating sphere. The Lambda-12, which is used to determine $a_{ys}(z_d,\lambda)$, is suitable for absorbance measurements using 10 cm cuvettes. Both systems can cover an extended spectral interval ranging from the ultraviolet to

---

† Milli-Q is a trademark of the Millipore Corporation (Bedford, Massachusetts).

the near-infrared. The spectrometers were operated with the UV WinLab software (version 2.80.03).

1.5 BIOGEOCHEMICAL ANALYSIS

Relevant biogeochemical seawater components, such as the concentrations of phytoplankton pigments C_{pig} and of total suspended matter, C_{TSM}, were determined for each measurement station from the water samples analysis.

1.5.1 HPLC System

The phytoplankton pigment concentration C_{pig} was determined using an Agilent† 1100 series HPLC system composed of a reverse phase C_{18} column (with a C_{18} guard column), an autosampler (with thermostat), a diode array detector (DAD), a fluorescence detector, and a three-solvent gradient. The system was operated with the Agilent Chemstation software (revision A.09.01).

1.5.2 Electrobalance

The concentration of TSM was measured by weighing the deposit on Millipore glass fiber filters (GF/F) with $0.7\,\mu\text{m}$ average pore size, by using an electrobalance with an accuracy greater than $0.1\,\text{mg}$.

1.6 ATMOSPHERIC INSTRUMENTS

The atmospheric optical measurements collected during the CoASTS campaigns were a) the direct solar irradiance, $E(\lambda)$; b) the diffuse sky radiance, $L_i(\theta, \phi, \lambda)$, at solar zenith angle θ and azimuth angle ϕ; and the total and diffuse solar irradiances, $E_d(0^+, \lambda)$ and $E_i(0^+, \lambda)$, respectively.

1.6.1 CE-318 Sun Photometer

The direct solar irradiance and the sky radiance in a wide range of angles in the almucantar and in the sun planes were both measured with a CE-318 automatic sun photometer. The instrument is composed of a) a sensor installed in an alto-azimuthal platform, b) a programmable

unit controlling measurement sequences plus data logging, and c) a data transmission unit based on the Meteorological Satellite (METEOSAT) Data Collection Platform (DCP) system. The optical part of the CE-318 is composed of two collimators with $1.2°$ FAFOV, one used for $L_i(\theta, \phi, \lambda)$ and the other used for both $E(\lambda)$ and $L_i(\theta, \phi, \lambda)$ in the sun aureole, plus a filter wheel with seven filters in the 412–1,020 nm spectral range.

1.6.2 Shadow Band

The $E_d(0^+, \lambda)$ measurements were collected using an OCI-200 radiometer. The $E_i(0^+, \lambda)$ irradiances were measured with the same radiometer by shading the direct sun irradiance component. The shading was obtained using a rotating shadow band attachment manufactured by Satlantic (Hooker and Lazin 2000). This device was remotely operated at the end of each measurement station, to shade the irradiance collectors through an automated arc-shaped shadow band moving above the radiometer.

1.7 ANCILLARY INSTRUMENTS

Additional instruments used within the CoASTS campaigns are a CTD for the characterization of seawater salinity $S_s(z)$ and temperature $T_s(z)$, and meteorological instruments.

1.7.1 CTD

Salinity and temperature profiles were produced using an OS-401 manufactured by IDRONAUT (Brugherio, Italy). The data logging was made using the OS-401 software (version 1.0) provided by the manufacturer.

1.7.2 Meteorological Instruments

The meteorological instruments, which are permanently mounted on the uppermost deck of the AAOT, were manufactured by SIAP‡ (Bologna, Italy) and were used to measure the wind speed and direction, atmospheric pressure, air temperature, and relative humidity.

---

† Formerly the Hewlett-Packard Analytical Division.

‡ *Societa Italiana Apparecchi di Precisione.*

Chapter 2

The Horizontal Deployment System (HDS)

Dirk van der Linde
JRC/IES/Inland and Marine Waters Unit
Ispra, Italy

Abstract

The HDS was primarily designed to support investigations for determining tower perturbations in above-water radiometric measurements. The system consists of a tubular horizontal mast sliding within rigidly mounted support frames. The mast is 21 m long and is composed of eight aluminum trusses plus a specially designed terminal end for affixing an instrument package. Each support frame encloses the mast with eight rollers with stainless steel bearings and permits the mast to be moved by a single operator. The HDS has the capability of carrying an instrument package weighing approximately 10 kg, and to deploy it up to as much as 12 m away from the main tower superstructure with a vertical deflection of the mast less than 1% (i.e., less than a 10 cm drop in the vertical for a 10 m extension in the horizontal).

2.1 INTRODUCTION

The determination of tower perturbations on above-water radiometric data, requires an analysis of superstructure effects as a function of the displacement distance between the platform and the area on the sea surface observed by the radiometer (the so-called *surface spot*). Because the measurement method requires a specific geometry between the radiometers and the sun, the displacement distance is a function of the sun zenith angle, the sensor viewing angle, the relative sun–sensor azimuth angle, and the deployment height and distance of the above-water radiometer.

To ensure an extensive analysis of the AAOT perturbation effects on above-water radiometric measurements, an extensible system was designed to position an instrument package weighing approximately 10 kg up to 12 m from the main tower superstructure (van der Linde 2003). The system was designed to provide an easy and quick repositioning of the sensor package at predefined distances from the superstructure, with a vertical flexion of the horizontal mast of less than 1% (i.e., less than a 10 cm deflection in the vertical direction for a 10 m extension in the horizontal).

2.2 DESCRIPTION

The HDS is composed of a horizontal mast made of eight truss sections and five support frames (Fig. 8). The mast can be moved in the horizontal direction by sliding it over a set of rollers mounted along the inner housing of the support frames. The eight interconnected truss sections,

plus a special 1 m long terminal element, yields an overall length of 21 m. The terminal end was designed to hold the above-water instrument package (Fig. 2 inset). The shape and size of the terminal element ensures a minimum perturbation to the radiometers installed on the mounting arm. The complete horizontal mast was treated with a primer, and then painted flat black.

The aluminum truss sections (Fig. 9) were manufactured by Trabes (type Professional 30, model quadro†), and are 2.5 m long, with a main tube thickness of $50{\times}2$ mm and a diagonal tube thickness of $20{\times}2$ mm. The trusses are made of 6082 T-6 aluminum for which the technical characteristics are outlined in *Deutsche Industrie-Normen‡* (DIN) 1748.

The interconnecting elements of the mast sections are welded to the four main tubes of each mast. The sections are connected to each other through a special coupler system. As shown in Fig. 9, the terminals of the main tubes of each section have an aluminum insert (C) that is pressed into the tube and then crimped to keep it in place. Solid aluminum double conical couplers (D) are set into the inserts of the mast sections and blocked by conical pins (E), which are hammered into place and secured with spring clasps.

The mast support frames (Fig. 10) were designed to hold a total weight of 150 kg and provide an easy manual

---

† Commercialized by MG S.r.l. (Roncadello, Italy).

‡ The German industry standards, which are a set of standards for industrial products established by the *Deutscher Normenausschuss*, a German organization for the establishment and registration of standards in all branches of industry.
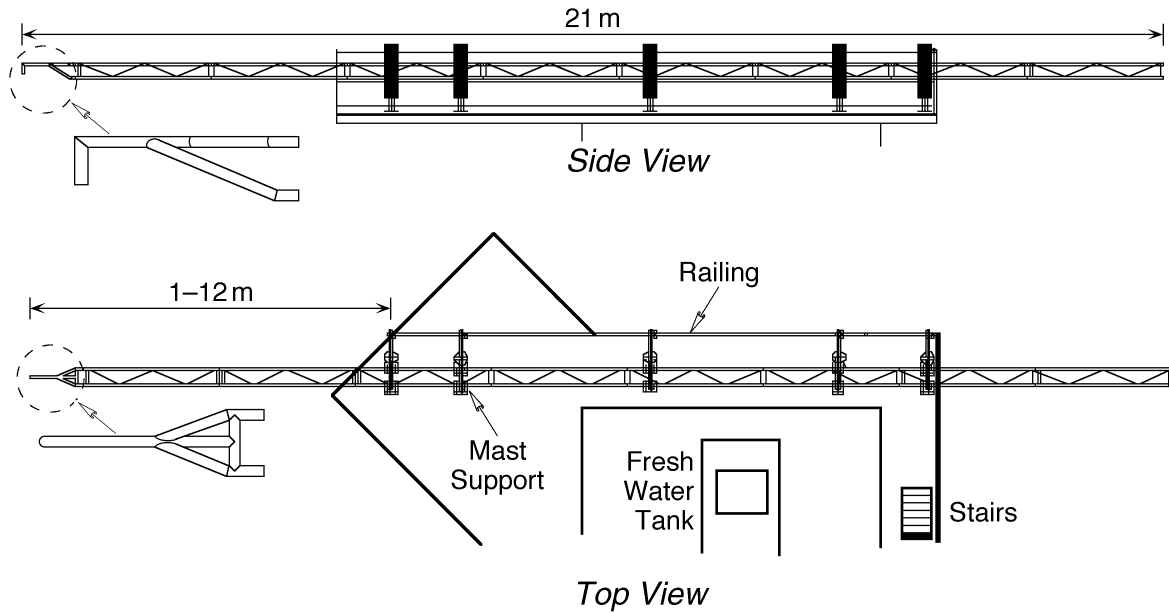
Fig. 8. The HDS installed on the top-most deck of the AAOT shown schematically as a side view (top drawing) and a top view (bottom drawing). The terminal end for mounting the microSAS radiometer system is shown in magnified detail for each view. The five support frames are affixed to the side railing of the platform. The mast can be extended 1–12 m over the side of the tower (with respect to the first mast support frame). Although arbitrary distances are possible, the mast was marked in integer reference distances of $0, 1, 2, \ldots, 12$ m to provide a simple and accurate repositioning capability.
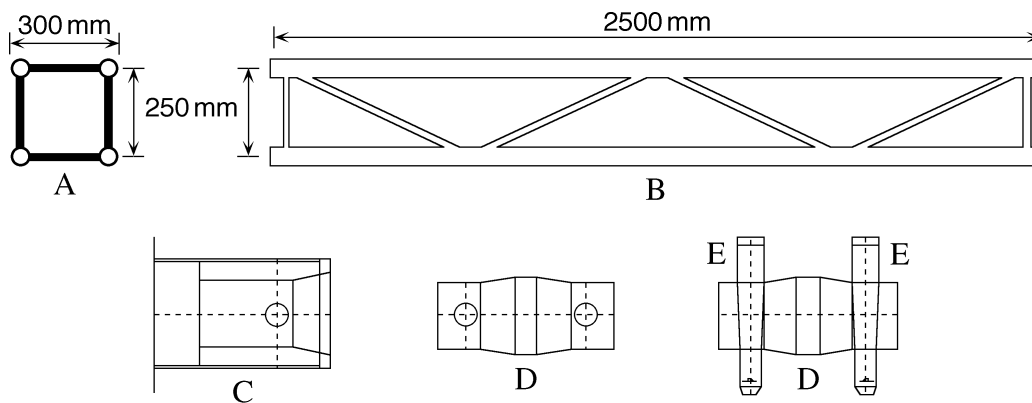
Fig. 9. A cross section (A) and side-view schematic of a tubular aluminum truss section (B) along with the components used to join the sections together to form the movable mast (Fig. 8). The ends of the main tubes of each section have an aluminum insert (C) that is pressed into the tube and crimped into place. Solid aluminum double conical couplers (D) are set into the inserts of the mast section and blocked by conical pins (E), which are hammered into place and secured with spring clasps (not shown here).

sliding of the horizontal mast, so it could be manipulated for a single operator. Each support frame encloses the mast with eight poliammide (82 mm×60 mm) rollers with stainless steel bearings. The rollers are set in rigid square supports made out of IPE100 steel (DIN 1025). The distance from the rollers to the mast section is adjustable. The supports are made of steel (Fe 3608 UNI 7070), treated with a primer and painted flat black. Each support frame is supported by two adjustable feet 250 mm high, which are bolted to the deck. The whole system is connected, on one side, to the AAOT railing through 50 mm diameter (angle-adjustable) scaffolding clamps. Prior to the final tightening of the scaffolding clamps, the mast support frames were leveled and aligned to avoid any strain to the horizontal mast during use.
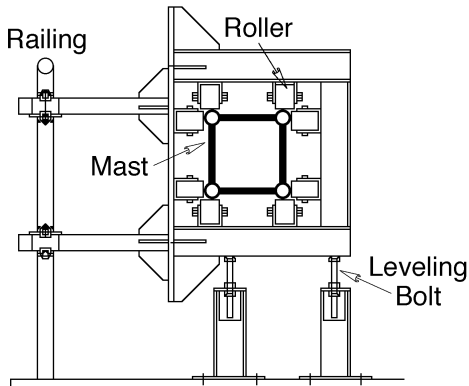
Fig. 10. A schematic of the horizontal mast support frame. The eight rollers support the mast as it is slid horizontally through the support frame.

The flexion, F_t, of the mast at the mounting point of the instrument package is a function of the distance, D_i, between the instrument mounting point and the nearest support frame. Mast deflections with respect to the horizontal level are caused by the weight of the instrument package plus that of the mast itself. Values of F_t as a function of the displacement distance, D_i, of the mast are given in Table 3 for the maximum load, L_D, applicable at the instrument mounting point (the terminal end of the mast).

Table 3. Flexion values F_t of the mast for a load L_D at distance D_i.

D_i [m]	L_D [kg]	F_t [cm]
1	1,663	0.4
2	831	1.7
3	554	3.8
4	416	6.8
5	300	9.7
6	171	10.0
7	100	10.0
8	59	10.0
9	21	10.0
10	15	10.0

Because the whole system was assembled together, distance markers were placed on the horizontal mast for a quick determination of its relative position with respect to the tower. A special mark was set at 12 m to remind the operator as to the maximum safe extension of the mast. At the other extreme of the mast, a scaffolding clamp was placed to prevent an accidental extension of the mast beyond the 12 m mark.

During each positioning sequence, the power and telemetry cables from the microSAS sensors needed to be manually fed onto, or retrieved from, the mast structure as the mast was extended or recovered, respectively. In practice, this did not prevent a rapid positioning of the mast, because the operator could move the mast with one hand while using the other to feed or store the cables.

2.3 SUMMARY

The HDS is one of the deployment systems designed for the AAOT to support recurring activities for the development and validation of ocean color products as well as specialized field experiments, like the tower-perturbation measurements. Its major feature is to ensure the deployment of a sensor package of approximately 10 kg up to a distance of 12 m from the main AAOT superstructure using a tubular horizontal mast sliding within fixed support frames.

Chapter 3

In Situ Methods

Giuseppe Zibordi
Jean-François Berthon†
JRC/IES/Inland and Marine Waters Unit
Ispra, Italy

Stanford B. Hooker
NASA/Goddard Space Flight Center
Greenbelt, Maryland

Abstract

The *in situ* methods used during the tower-shading campaigns were a direct consequence of making above- and in-water measurements of the radiance field within the coastal ocean environment. The in-water measurements were intended as a *reference* or ground truth, because previous campaigns had established a methodology for correcting the in-water data for tower perturbation effects. Much of the above-water experiments, however, were by definition degraded—they were specifically designed to capture the perturbation of the tower in the surface radiance field. The spatial complexity (primarily vertically for the duration of the experiments considered here) of the coastal ocean makes the interpretation of optical profiles alone very difficult, so a variety of supporting measurements and methods were used to produce a thorough description of the vertical properties of the water column.

3.1 INTRODUCTION

The *in situ* methods considered here are those directly or indirectly used for investigating above-water tower perturbations in the coastal ocean. The distinction between primary and secondary measurements is made, because a full understanding of the variance in the data frequently requires ancillary data not used in the principal analytical variables. One of the advantages of executing the tower-perturbation campaigns at the AAOT was the immediate access to a comprehensive set of environmental data products without the need for adding additional instruments or personnel.

3.2 AOP METHODS

The design and use of the AOP instruments are inexorably tied to the basic equations relating the upward radiance field below the surface with that exiting the surface, the angular bidirectional dependency of these fields, and the transformation of radiance or irradiance into reflectance. The full set of these equations are detailed in

Morel and Gentili (1996) and in Mobley (1999) as well as the most recent version of the protocols for above- and in-water radiometry (Mueller and Morel 2002), so only brief summaries are considered here.

The spectral radiance emerging immediately above the ocean (at a depth denoted $z = 0^+$), the so-called *water-leaving radiance*, for a given solid angle of the detector, Ω_{FOV}, is a function of the azimuthal and zenith viewing angles of the instrument with respect to the azimuthal and zenith angle of the sun. For brevity, the explicit presentation of Ω_{FOV} and the angular geometries is not repeated hereafter except where needed to clarify specific details of the methods involved.

The illumination conditions above the sea surface depend on a direct component from the sun and a diffuse component from the sky. In addition to the sun position in a cloudless sky, the aerosol nature and optical thickness determine the radiant field above the ocean, and then subsequently the upward radiance field inside the ocean. In the case of partly cloudy skies, the radiant field is more complex, because it depends on the cloud type and distribution. For the above- and in-water methods considered in this study, the above-surface illumination is expressed in a simplified way by only considering the solar zenith angle (and the measurements are made during predominantly clear-sky conditions).

---

† Currently with *Université du Littoral Côte d'Opale* (ULCO) *Maison de la Recherche en Environnement Naturel* (MREN), Wimereux, France.

3.2.1 In-Water Methods

At a depth z within the water, the upwelled radiance measured by a nadir-viewing sensor is denoted $L_u(z, \lambda)$, where the dependence on the illumination conditions prevailing above the sea surface is omitted for brevity. At a null depth, denoted $z = 0^-$ by convention, the water-leaving radiance, L_W, is related to the upwelled nadir radiance by the (upward) radiance transmittance, $T_0(\lambda)$ through the air–sea interface:

$$L_W(0^+, \lambda) \ = \ T_0(\lambda) \, L_u(0^-, \lambda), \tag{1}$$

where $T_0 = \left[1 - \rho(\lambda)\right] n^{-2}(\lambda)$, n is the refractive index of seawater, and ρ is the (upward) Fresnel reflectance coefficient (Austin 1974). For the wavelengths considered here, n and ρ are essentially constant and the wavelength dependence is no longer repeated.

When using an in-water method, a vertical profile of L_u within the upper layer is usually determined with a radiometer pointed at nadir. By using the diffuse attenuation coefficient associated with the upwelled radiance, (K_L), the $L_u(0^-, \lambda)$ value at null depth is derived by extrapolating the profile toward the interface. This radiance is then propagated through the interface using (1), with T_0 given a constant value (because n and ρ are now assumed constant) of $T_0 = 0.544$, which has a nearly constant value regardless of the sea state (Austin 1974 and Mobley 1999). Defining now that all L_W values are at $z = 0^+$, and that the water-leaving radiance from an in-water measurement is represented by $\tilde{L}_W$,

$$\tilde{L}_W(\lambda) \ = \ 0.544 \, L_u(0^-, \lambda). \tag{2}$$

The upward radiance is related to the upward irradiance, E_u, at the same depth (at 0^-, for example), through

$$L_u(0^-, \lambda) \ = \ \frac{E_u(0^-, \lambda)}{Q(0^-, \lambda)}, \tag{3}$$

where the bidirectional Q function is expressed in steradians (it would be exactly equal to π if the L_u field was isotropic). By introducing the irradiance reflectance, denoted R, E_u can be expressed as a function of the downward irradiance, E_d, just beneath the surface through

$$E_u(0^-, \lambda) \ = \ R(\lambda) \, E_d(0^-, \lambda). \tag{4}$$

The remote sensing reflectance, $R_{\rm rs}$, is defined as the ratio of the water-leaving radiance originating from nadir to the downward irradiance above the surface, $E_d(0^+, \lambda)$:

$$R_{\rm rs}(\lambda) \ = \ \frac{L_W(\lambda)}{E_d(0^+, \lambda)}, \tag{5}$$

so it can be easily derived from an in-water radiance measurement.

Finally, it is worth recalling that the so-called *normalized water-leaving radiance* (Gordon and Clark 1981) is defined as the hypothetical water-leaving radiance that would be measured if the sun was at the zenith, and in the absence of any atmospheric loss:

$$\left[L_W(\lambda)\right]_{\rm N} \ = \ F_0(\lambda) \, R_{\rm rs}(\lambda), \tag{6}$$

where $F_0(\lambda)$ is the spectral value of the extraterrestrial solar flux (Neckel and Labs 1984) when the Earth is at its mean distance from the sun.

The formulations in (2)–(6) dictate the sensors needed to derive the water-leaving radiance and the normalized forms thereof. Traditionally, this has been accomplished with integrated optical systems deployed using a winch and crane. The problem with such an approach is it is difficult to get the optical instrumentation far enough away from the sampling platform to ensure the data are not contaminated by perturbations (shading, reflections, etc.) associated with the platform. In addition, integrated systems are not easily serviced in the field if problems arise—spare components are not easily swapped for malfunctioning ones without compromising the calibration of the light sensors.

3.2.2 Above-Water Methods

When using an above-water method, the total radiance above the sea surface, L_T, measured at a nadir angle ϑ and an azimuthal angle ϕ' with respect to the solar azimuth (ϕ) includes the wanted water-leaving radiance (1), and a contamination term, ΔL originating from light reflected onto the sea surface and then into the field of view (FOV) of the sea-viewing sensor,

$$L_T(0^+, \lambda, \phi', \vartheta) \ = \ L_W(0^+, \lambda, \phi', \vartheta) \ + \ \Delta L, \tag{7}$$

where, again, the solar geometry is omitted for brevity. According to the latest version of the SeaWiFS Ocean Optics Protocols (Mueller et al. 2002) and simulations by Mobley (1999), ϑ is usually chosen between 20–50° (here 40°), and ϕ' is generally between 90–135°, away from the solar azimuth (here either 90° or 135°).

The water-leaving radiance in (7) can only be obtained by correctly removing the contamination term, ΔL, which is composed primarily (in clear-sky conditions) of sun and sky glint. There are several techniques for removing sky glint (e.g., Morel 1980, Carder and Steward 1985, and Lazin 1998) The method considered here is the so-called *modified Fresnel reflectance glint correction* as presented in the version 1 revision of the SeaWiFS Ocean Optics Protocols (Mueller and Austin 1995), hereafter referred to as S95. In this formulation

$$\Delta L \ = \ \rho \, L_i(\lambda, \theta, \phi', \vartheta'), \tag{8}$$

where ϑ' is the zenith angle equivalent of the ϑ nadir angle $(\vartheta' = 180 - \vartheta)$. The reflectance factor ρ would be the

Fresnel reflectance averaged over the FOV of the detector if the interface was level. This is usually not the case, so ρ depends on the solar geometry (θ, ϕ) and the capillary wave slopes, and, thus, on wind speed, W (Austin 1974 and Mobley 1999). It is worth noting an extraneous source of reflected light (e.g., from the measurement platform) is, by definition, assumed negligible when using the S95 method.

The original S95 specifications recommended a pointing angle $\vartheta = 20°$ from nadir (Mueller and Austin 1995). Radiative transfer simulations above a wave-roughened surface from Mobley (1999) showed a superior angle was $40°$, and that a preferred azimuth angle was $135°$. With these viewing angles, the reflectance factor ρ amounts to 0.028 for $W < 5\,\mathrm{m\,s^{-1}}$, and increases up to about 0.04 when $W = 15\,\mathrm{m\,s^{-1}}$. The S95 method used a constant $\rho = 0.028$ value and, thus, was only valid at low wind speeds.

Sun glint can be minimized by pointing the radiometer at least $90°$ away from the solar azimuth, and then aggressive filtering can be used to remove any remaining glint in the data. Hooker et al. (2002a) demonstrated that if the radiometrically lowest (darkest) 5% of the data, based on the reddest band are kept, the best statistical agreement and flexibility is achieved. Application of this new filter is referred to hereafter as the S01 method.

3.3 IOP METHODS

Within the CoASTS measurement activities, the characterization of seawater IOPs was focused on the determination of $a(z, \lambda)$, $c(z, \lambda)$, and $b_b(z, \lambda)$ profiles through commercially available instruments. In addition, $a_{ph}(z_d, \lambda)$, $a_{dp}(z_d, \lambda)$, and $a_{ys}(z_d, \lambda)$ were separately determined from discrete water samples taken at fixed depths z_d (i.e., surface, 8 m and 14 m depth).

3.3.1 Beam Attenuation and Absorption

The coefficients $c(z, \lambda)$ and $a(z, \lambda)$ were computed from calibrated beam attenuation and absorption coefficients, $\hat{c}_{t-w}(z, \lambda)$ and $\hat{a}_{t-w}(z, \lambda)$, respectively, obtained from the AC-9 measurements for suspended and dissolved optical components (not including the contribution of pure seawater). The calibrated coefficients were corrected for salinity and temperature differences between the *in situ* seawater and the pure water used for laboratory calibration, using the CTD profile data (WETLabs 2002).

The measured beam attenuation coefficients corrected for salinity and temperature effects do not require any further processing, that is,

$$c(z, \lambda) = \hat{c}_{t-w}^{ST}(z, \lambda) + c_w(\lambda), \qquad (9)$$

where the ST superscript denotes the salinity and temperature correction, and $c_w(\lambda)$ is the beam attenuation coefficient for pure water.

The calibrated absorption coefficients need to be further corrected for scattering effects, because the finite acceptance angle of the optics and the incomplete reflectivity of the absorption tube surface prevents the detector from collecting all the scattered light, which induces an overestimate of the retrieved absorption coefficient. In the specific case of the CoASTS campaigns, these perturbation effects were removed using the method proposed by Zaneveld et al. (1994).

The Zaneveld et al. (1994) method is based on the removal of a variable percentage of the scattering coefficient estimated as the difference between $\hat{c}_{t-w}^{ST}(z, \lambda)$ and $\hat{a}_{t-w}^{ST}(z, \lambda)$. The method assumes the absorption coefficient of particulate and dissolved material is zero at a reference wavelength, $\lambda_0 = 715\,\mathrm{nm}$, and the shape of the volume scattering function is independent of wavelength, which means

$$a(z, \lambda) = \hat{a}_{t-w}^{ST}(z, \lambda) + a_w(\lambda) - \breve{a}_{t-w}^{ST}(z, \lambda_0), \qquad (10)$$

where $a_w(\lambda)$ is the absorption of pure water taken from Pope and Fry (1997) and

$$\breve{a}_{t-w}^{ST}(z, \lambda_0) = \hat{a}_{t-w}^{ST}(z, \lambda_0) \frac{\hat{c}_{t-w}^{ST}(z, \lambda) - \hat{a}_{t-w}^{ST}(z, \lambda)}{\hat{c}_{t-w}^{ST}(z, \lambda_0) - \hat{a}_{t-w}^{ST}(z, \lambda_0)}. \qquad (11)$$

3.3.2 Backscattering

The determination of $b_b(z, \lambda)$ with the HYDROSCAT-6 instrument is based on the assumption that it is correlated with backscattering measurements at $140°$, where the shape of the volume scattering phase function has the least variability. A comprehensive description of the measurement principles and calibration requirements for the HYDROSCAT-6, are given in Maffione and Dana (1997).

3.3.3 Particulate Matter Absorption

The determination of the particulate matter absorption coefficients is made through spectrometric techniques applied to the deposit (by filtration) of particles on glass fiber filters with a nominal pore size of $0.7\,\mu\mathrm{m}$. The total absorption coefficient, $a_p(\lambda)$, of the equivalent particle suspension in the 400–750 nm spectral range (with 1 nm resolution) was computed according to

$$a_p(\lambda) = 2.3\,A_{\mathrm{sus}}(\lambda)\,\frac{F_a}{V_w}, \qquad (12)$$

where V_w is the volume of filtered water (in units of cubic meters), F_a is the filter clearance area (in units of square meters), and $A_{\mathrm{sus}}(\lambda)$ is the equivalent particle suspension absorbance obtained from the transmission and reflection method proposed by Tassan and Ferrari (1995), which has been shown to be appropriate for the analysis of water samples characterized by highly backscattering mineral particles or by highly absorbing sediments.

The two components $a_{ph}(\lambda)$ and $a_{dp}(\lambda)$ of the particulate absorption coefficient for the pigmented and non-pigmented fractions, respectively, were obtained through

bleaching of the sample on the filter using a solution of sodium hypochlorite (NaClO) as an oxidizing agent (Ferrari and Tassan 1999). This oxidation acts rapidly on pigment molecules and slowly on detritus, thereby permitting a selective analysis of the absorption components of non-pigmented particles retained on the filter.

3.3.4 CDOM Absorption

The coefficient $a_{ys}(\lambda)$ was obtained through spectrometric analysis of seawater filtered on 0.22 µm cellulose filters. The analysis was performed by placing a 10 cm quartz cuvette containing Milli-Q water in the optical path of the reference beam, and a 10 cm quartz cuvette containing the filtered seawater sample in the optical path of the sample beam. The spectral absorption coefficient $a_{ys}(\lambda)$ was computed from the measured absorbance $A_{ys}(\lambda)$ resulting from the difference between the sample absorbance and the reference absorbance (Ferrari et al. 1996), from

$$a_{ys}(\lambda) \ = \ 2.3 \, \frac{A_{ys}(\lambda)}{L_c}, \tag{13}$$

where L_c is the path length of the cuvette (in units of meters). The instrument background was removed using measurements performed with Milli-Q water in both the sample and the reference cuvettes.

3.4 BIOGEOCHEMICAL METHODS

Biogeochemical methods were restricted to the determination of pigments and total suspended matter concentrations on water samples taken at discrete depths. The pigments were determined using an HPLC method which quantitated the following pigments:

- Alloxanthin,
- Chlorophyll a,
- Chlorophyll b,
- Chlorophyll $c_{1 + 2}$,
- Chlorophyllide a,
- Diadinoxanthin,
- Diatoxanthin,
- Fucoxanthin,
- Zeaxanthin,
- 19′-butanoyloxyfucoxanthin,
- 19′-hexanoyloxyfucoxanthin, and
- $\beta\beta$-carotene.

3.4.1 Pigment Concentration

The applied HPLC method (Hooker et al. 2000b) follows the Joint Global Ocean Flux Study (JGOFS) core measurements protocols (JGOFS 1994) and is a modified version of the method presented by Wright et al. (1991).

The method does not permit the separation of divinyl chlorophyll a and of divinyl chlorophyll b from chlorophyll a and chlorophyll b, respectively. It was mostly used for Adriatic Sea waters, however, and because prochlorophytes are not found in coastal areas, its validity is not diminished. Filter disruption is accomplished mechanically using a motorized grinder. The pigments are extracted within a 100% acetone solution including an internal standard (*trans-β-apo-8′-carotenal*). The method provides measurements of the main pigment concentrations with a detection limit of approximately $1 \, \text{ng L}^{-1}$. The standard pigments and their extinction coefficients, used for the system calibration, were provided by the DHI Water and Environment Institute (Høsholm, Denmark).

3.4.2 TSM

The concentration of total suspended matter, C_{TSM}, was obtained from the net weight of the material collected on GF/F filters following a slightly modified version of the method proposed by Strickland and Parsons (1972). Seawater samples were filtered through prewashed, preashed, and preweighed filters. After filtration, the filter (filtration area and border) was washed with distilled water and stored at $-18°$C. Before final weighing, the filters were dried at $75°$C for 1 h, and then temporarily stored in a desiccator. The value of C_{TSM} (in units of grams per liter) was calculated from

$$C_{\text{TSM}} \ = \ \frac{W_s \ - \ W_f \ - \ \bar{w}_b}{V_w}, \tag{14}$$

where W_f is the weight of the filter before filtration, W_s is the weight of the sample filter after filtration, V_w is the volume of the filtered water, and $\bar{w}_b$ is a correction term introduced to account for changes in the weight of the filter sample because of changes caused by environmental conditions and handling in between the two weighing steps.

3.5 ATMOSPHERIC METHODS

The atmospheric measurements were acquired to characterize the optics of the atmosphere during the execution of station measurements. Specifically, they were focused on determining the aerosol optical thickness and the ratio of the diffuse-to-direct solar irradiance. The latter has relevance for the removal of instrument self-shading effects and tower-shading perturbations (in the specific case of WiSPER data) for in-water optical measurements (Zibordi et al. 2002a).

3.5.1 Aerosol Optical Thickness

The aerosol optical thickness, $\tau_a(\lambda)$, was determined from $E(\lambda)$ taken at air mass m in the range 440–1,020 nm (Holben et al. 1998). Assuming no water vapor absorption,

$E(\lambda)$ is related to the atmospheric optical thickness, τ, through

$$E(\lambda) \; = \; E_0(\lambda) \, D \, e^{-\tau(\lambda)m}, \qquad (15)$$

where $E_0(\lambda)$ is the extra-atmospheric irradiance, D is the sun–Earth distance correction factor, and $\tau(\lambda) = \tau_R(\lambda) + \tau_o(\lambda) + \tau_a(\lambda)$, i.e., the sum of the Rayleigh, ozone, and aerosol optical thicknesses, respectively).

3.5.2 Diffuse-to-Direct Irradiance Ratio

The diffuse-to-direct irradiance ratio, $r_d(\lambda)$ was computed from $E_d(0^+, \lambda)$ and $E_i(0^+, \lambda)$ according to

$$r_d(\lambda) \; = \; \frac{E_i(0^+, \lambda)}{E_d(0^+, \lambda) \; - \; E_i(0^+, \lambda)}. \qquad (16)$$

The $E_i(0^+, \lambda)$ data were collected by occulting the $E_d(0^+, \lambda)$ sensor (Figs. 3 and 4). Although the $E_d(0^+, \lambda)$ sensor was calibrated to ensure accurate normalization of the in-water optical data, the computation of $r_d(\lambda)$ derived from the same instrument does not require an absolute radiometric calibration.

3.6 ANCILLARY METHODS

Meteorological and CTD data, along with generic observations (like sea state and cloud cover), complete the list of measurements taken during the CoASTS measurement stations.

3.6.1 Hydrographic Data

The salinity and temperature data were produced from CTD profiles taken during each station with the objective of characterizing the seawater and providing data for the AC-9 temperature and salinity corrections.

3.6.2 Meteorological Data

For each CoASTS measurement station, the major meteorological quantities were recorded including atmospheric pressure, relative humidity, air temperature, wind speed, and wind direction. In addition, the Secchi depth was recorded together with the sea state, as defined by the World Meteorological Organization (WMO) code (WMO 1983), and the cloud coverage (in quarters).

Chapter 4

Advances in Data Processing Methods

Stanford B. Hooker
NASA/Goddard Space Flight Center
Greenbelt, Maryland

Giuseppe Zibordi
Davide D'Alimonte
JRC/IES/Inland and Marine Waters Unit
Ispra, Italy

James W. Brown
RSMAS/University of Miami
Miami, Florida

Abstract

New versions of the data processing methods were created to accommodate a) the incorporation of an automated system for determining the ratio of diffuse-to-direct solar irradiance, and b) the correction for bidirectional effects in the above-water (sea-viewing) measurements. The former required a more sophisticated correction to the occulted solar reference data, and the latter required a more complete formulation of the above-water method. Neither advancement altered the type of data collected or the basic data collection methodology.

4.1 INTRODUCTION

The primary advances in data processing during the time period covered by the tower-perturbation campaigns were a consequence of a) replacing the manual occulting of the global solar irradiance with an automated capability (a variant of SeaSHADE), and b) including a more complete correction for bidirectional effects in the above-water (sea-viewing) measurements.

4.2 THE IRRADIANCE RATIO

Estimating the magnitude of perturbations in underwater optical measurements from instrument self-shading and large deployment structures (ships and towers) requires information on the sky radiance distribution. The computation of sky radiance requires an accurate knowledge of atmospheric optical parameters (i.e., the scattering phase function and optical thickness) and the use of exact radiative transfer codes. Computations for cloudy conditions, however, may be affected by large uncertainties. Because of this, operational correction schemes for the removal of self-shading and platform perturbations were proposed by parameterizing the effects of sky radiance distribution with the diffuse-to-direct downward irradiance ratio $r_d(\lambda)$ (Gordon and Ding 1992 and Doyle and Zibordi 2002).

The determination of $r_d(\lambda)$ is possible using irradiance sensors by collecting the total $E_d(0^+, \lambda)$ and the diffuse $E_i(0^+, \lambda)$ downward irradiance. In most cases, $E_i(0^+, \lambda)$ measurements are acquired by shading the direct sun irradiance component with an occulter (usually a wand-shaped device resembling a lollipop) manually placed at some distance from the collector(s) of the radiometer such that the shadow from the occulter completely shades the diffuser(s).

The difficulty with manually occulting solar references is the sensors are frequently placed in difficult access locations on many ships, so data collection is usually not convenient and in many circumstances hazardous (even with a safety harness). An alternative to the manual solar occulter is provided by radiometers equipped with rotating shadow bands autonomously occulting the global (direct plus diffuse) sun irradiance (Guzzi et al. 1985 and Harrison et al. 1994).

Based on an automated occulting principle, SeaSHADE was developed to autonomously measure $E_i(0^+, \lambda)$ with the same radiometer used for measuring $E_d(0^+, \lambda)$ during the collection of in-water optical profiles of $E_d(z, \lambda)$, $E_u(z, \lambda)$, and $L_u(z, \lambda)$ (Hooker and Lazin 2000). The SeaSHADE occulting element is a hemispherical band moving at a constant speed over the top of the irradiance sensor and blocking a portion of the sky with approximately a $7°$ angle.
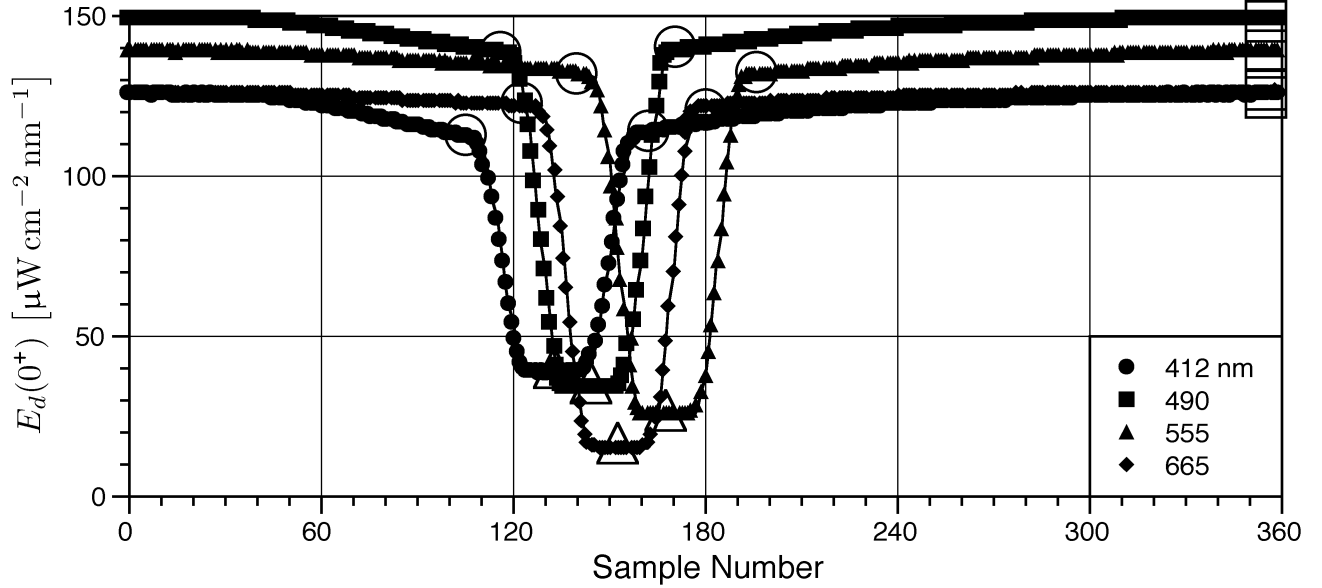
Fig. 11. A plot of a shadow band data acquisition sequence for four wavelengths. The $E_d(0^+)$ maximum values for the measured solar irradiance for each channel are given by the open squares, the $\hat{E}_i(0^+)$ minimum values by the open triangles, and the $E_b(0^+)$ band correction values by the open circles.

In the idle (or home) position, at one terminus of the sensor, the band does not shade or perturb the $E_d(0^+, \lambda)$ measurements. During the angular sweep from one side to the other, the band progressively occults the sun. When the sun is completely occulted $E_i(0^+, \lambda)$ is measured, but this measurement includes a perturbation caused by the band blocking a portion of the sky radiance field. This latter term is denoted, $E_b(0^+, \lambda)$, and must be included in reconstructing the true $E_i(0^+, \lambda)$ values:

$$E_i(0^+, \lambda) = E_d(0^+, \lambda) - \left[E_b(0^+, \lambda) - E_m(0^+, \lambda)\right], \quad (17)$$

where $E_m(0^+, \lambda)$ is the measured (minimum) irradiance when the sun is occulted.

Different methods were proposed to quantify $E_b(0^+, \lambda)$ from the irradiances measured during the rotation of the band (Bonzagni et al. 1989). In agreement with Harrison et al. (1994), $E_b(0^+, \lambda)$ can be evaluated from the irradiance measurements taken just before and just after the band shades the diffuser(s). Based on this principle, a processing scheme was developed to determine $r_d(\lambda)$ from SeaSHADE measurements. The value of $r_d(\lambda)$ is computed using

$$r_d(\lambda) = \frac{E_d(0^+, \lambda) - \left[E_b(0^+, \lambda) - E_m(0^+, \lambda)\right]}{E_b(0^+, \lambda) - E_m(0^+, \lambda)}, \quad (18)$$

where the numerator is the diffuse sky irradiance and the denominator is the direct sun irradiance.

The value of $E_b(0^+, \lambda)$ is taken as the average irradiance immediately before and after the band shades the diffuser. The two irradiance values for computing $E_b(0^+, \lambda)$ are those acquired at the times $t_0 \pm \Delta t$, were t_0 is the time corresponding to the minimum of the measured irradiance values during the band rotation period $\left[\text{i.e., } E_m(0^+, \lambda)\right]$ and the increment Δt is experimentally determined.

The computation of $r_d(\lambda)$, being made with a single radiometer and based on ratios, does not require an absolute radiometric calibration. During clear-sky conditions at the AAOT site, the $r_d(\lambda)$ values typically range within 0.89 ± 0.41 at 412 nm (Zibordi et al. 2002a), while during overcast conditions $r_d(\lambda) \to \infty$. Figure 11 shows the irradiance data collected at the AAOT for a half-cycle rotation of the band at 412, 490, 555, and 665 nm.

4.3 EXACT $[L_W]_N$ FORMULATION

Intercomparisons of above- and in-water determinations of water-leaving radiances, $\hat{L}_W(\lambda)$ and $\tilde{L}_W(\lambda)$, respectively, have been quantified using the relative percent difference (RPD). In these studies, $\tilde{L}_W(\lambda)$ is considered the reference value, and the RPD, $\psi(\lambda)$, is computed as

$$\psi(\lambda) = 100 \frac{\hat{L}_W(\lambda) - \tilde{L}_W(\lambda)}{\tilde{L}_W(\lambda)}. \quad (19)$$

Detailed intercomparisons of a variety of methods for determining water-leaving radiances by Hooker et al. (2002a) showed above-water values were recurringly larger—on the order of as much as 9%—than in-water determinations.

Using (7) and (8), the S95 method (and equivalently the S01 method) is given as

$$\hat{L}_W^{S95}(\lambda) = L_T(\lambda) - \rho L_i(\lambda), \quad (20)$$

where ρ is presented as a constant (0.028), and the pointing angles with respect to the sun (ϕ'), sea (ϑ), and sky

(ϑ') have been omitted for brevity. A positive bias in $\hat{L}_W$ values with respect to $\tilde{L}_W$ values can be explained by three possibilities: a) an overestimation of L_T, b) an underestimation of L_i, and c) an underestimation of ρ.

The L_T and L_i measurements are obtained using radiometers calibrated at the same calibration facility with a calibration uncertainty on the order of 2% (Hooker et al. 2002b). Furthermore, all the above- and in-water sensors are frequently intercalibrated to within 1% using a portable source or a common calibration process (Hooker et al. 2002a), so it is unlikely differences in the absolute measurement capabilities of the sensors can explain (approximately) a 9% bias.

The aforementioned aggressive filtering used with the S01 method removes elevated signals associated with glint spikes in the L_T observations, but these data are acquired at a viewing angle that is substantially different than the in-water viewing angle. The anisotropy of the radiance distribution field is a possible contributor to the bias, and has the anticipated effect as a function of the viewing angle, that is, as the viewing angle increases away from nadir, L_W increases with respect to the nadir value.

The L_i data are acquired using a calibrated radiometer under predominately clear-sky conditions, which minimizes the possibility nearby clouds would invalidate the L_i component to the sky glint correction. The contribution of ρ, however, is not correctly modeled as a constant and should include a wind speed dependence. As W increases, ρ increases, so a more accurate ρ value will frequently increase the magnitude of the sky glint correction term, which will reduce $\hat{L}_W$ and, thus, the positive bias.

The primary improvements in the above-water processing discussed here are a) a more accurate determination of the surface reflectance, ρ, and b) correcting $\hat{L}_W$ values for bidirectional effects, i.e., accounting for the angular dependence (anisotropy) of the in-water radiance field. The former is addressed here using the Mobley (1999) formulation for the effect of wind speed (plus the solar and sensor viewing geometry) on ρ to update the S01 method.

Assuming the unwanted ΔL term in (7) has been successfully removed with a more accurate surface reflectance and platform perturbations are not present, the problem considered next is how best to intercompare L_W values resulting from simultaneous above- and in-water measurements. Because the instrument pointing angles for in-water measurements are all approximately zero, Q in (3) takes a particular value, denoted $Q_n(0^-, \lambda, \theta)$ (for nadir-viewing), which still depends on the solar geometry. For above-water measurements, the angular parameters are imposed by the pointing angles of the sensors with respect to the sun, sea, and sky, as well as, the surface effects of reflection and refraction.

When dealing exclusively with Case-1 waters, the functional dependence of the variables can be simplified, in particular, it is (by definition) assumed that the IOPs are universally related to the chlorophyll a concentration, C_a

(Morel and Prieur 1977). Using this assumption and omitting the wavelength dependence plus the $z = 0^-$ notation for Q and Q_n (but reintroducing the solar and pointing geometry where explicitly useful for clarity), the ratio of the above- and in-water L_W quantities is given by (Morel and Mueller 2002):

$$\frac{\hat{L}_W(\phi', \vartheta)}{\tilde{L}_W} = \frac{\Re(\theta', W)}{\Re_0} \frac{Q_n(\theta, C_a)}{Q(\theta, \phi', \theta', C_a)}, \qquad (21)$$

where θ' is the above-water viewing angle refracted by the air–sea interface, the factor $\Re$ merges all the effects of reflection and refraction (the $\Re_0$ term is evaluated at nadir, i.e., $\theta' = 0$).

The above-water measurements collected at a particular viewing angle (e.g., $\vartheta = 40°$ which corresponds to $\theta' = 29°$), can be transformed on a case-by-case basis as if they were made vertically (at nadir). The simplest transformation makes use of Q-function look-up tables derived from calculations for a clear sky (Morel and Gentili 1996) and a constant surface transmission effect, that is, $\Re/\Re_0$ is a constant. In addition to the θ' and λ values, the Q-factor entries depend on the azimuth difference between the viewing and solar planes (ϕ'), and the chlorophyll a concentration.

The formulation in (21) shows Q corrections are needed to not only intercompare above- and in-water water-leaving radiances, but also to produce R_{rs} values from $\hat{L}_W$ observations. Combining (5), which is formulated for nadir (in-water) radiances (i.e., $\tilde{L}_W$), and (21) yields

$$R_{rs} = \frac{\Re_0}{\Re(\theta', W)} \frac{Q(\theta, \phi', \theta', C_a)}{Q_n(\theta, C_a)} \frac{\hat{L}_W(\phi', \vartheta)}{E_d(0^+)}. \qquad (22)$$

Using (6) with (22) yields the relationship between the above- and in-water normalized water-leaving radiances:

$$\left[\tilde{L}_W\right]_N = \frac{\Re_0}{\Re(\theta', W)} \frac{Q(\theta, \phi', \theta', C_a)}{Q_n(\theta, C_a)} \left[\hat{L}_W(\phi', \vartheta)\right]_N. \qquad (23)$$

The use of (23), but assuming $\Re_0/\Re$ is a constant and using the Mobley (1999) results for computing the surface reflectance for (8), is referred to hereafter as the Q01 method. This normalized quantity (23) still depends on the viewing geometry (ϕ', ϑ) and, thus, on the bidirectional properties of the water body. This dependence is removed through

$$\left[L_W\right]_N^{ex} = \frac{f_0(C_a)}{Q_0(C_a)} \left[\frac{f(\theta, C_a)}{Q_n(\theta, C_a)}\right]^{-1} \left[\tilde{L}_W\right]_N, \qquad (24)$$

where f is a function relating the irradiance reflectance (4) to the IOPs, and f_0 and Q_0 are defined for a zero sun zenith ($\theta = 0$) plus nadir viewing ($\theta' = 0$) for the latter.

Substituting (23) into (24) provides the transformation of the above-water signal into the exact normalized water-

leaving radiance:

$$\left[L_W\right]_{\mathrm{N}}^{\mathrm{ex}} \;=\; \frac{\Re_0}{\Re(\theta', W)} \frac{f_0(C_a)}{Q_0(C_a)} \left[\frac{f(\theta, C_a)}{Q(\theta, \phi', \theta', C_a)}\right]^{-1} \left[\hat{L}_W(\phi', \vartheta)\right]_{\mathrm{N}}. \tag{25}$$

The f/Q correction to the normalized water-leaving radiances for above-water measurements is implemented using the formulations and look-up tables presented by Morel et al. (2002). The latter, when compared to the Q01 method, gives a more accurate modeling of the surface transmission effects—the $\Re/\Re_0$ ratio has an angular and wind speed dependence, which also improves the accuracy of the water-leaving radiances (21) and remote sensing reflectances (22). The addition of this refinement to the Q01 method is referred to hereafter as the Q02 method.

Although the bidirectional correction associated with the Q02 method is more precise than the Q01 method, because of the more accurate surface transmission effects in the former, the differences between the two are usually small (less than 1%) for the solar geometry, the sensor sampling angles, and the environmental conditions encountered during the tower-perturbation campaigns. The most significant difference between the two is the exact formulation for the normalized water-leaving radiance in the Q02 method.

Chapter 5

Preliminary Results

STANFORD B. HOOKER
NASA/Goddard Space Flight Center
Greenbelt, Maryland

GIUSEPPE ZIBORDI
JRC/IES/Inland and Marine Waters Unit
Ispra, Italy

ABSTRACT

The analytical results are organized by separating the above-water radiometric data into near- and far-field categories. The former correspond to data for which $x < 13\,\mathrm{m}$, and the latter to data for which $x \geq 13\,\mathrm{m}$, where x is the perpendicular distance of the surface spot viewed by the sea-viewing sensor away from the tower. The far-field observations confirm uncontaminated above-water data can be collected in the vicinity of a large structure as long as the surface spot is as far away from the platform as it is high (in this case about $13\,\mathrm{m}$). The near-field data show significant perturbations, as much as 100% above far-field levels, which are substantially above any fluctuations that could be attributed to natural environmental variability (in the absence of floating material). A separate investigation of both the widespread and the sporadic effects of floating material showed perturbations as much as 25% above normal (uncontaminated) levels.

5.1 INTRODUCTION

Although in-water measurements have successfully been used for deriving water-leaving radiances and are recurringly used for validating ocean color sensors, above-water measurements form an alternative, which remain to be similarly exploited. From a measurement perspective, the above-water approach is more restrictive, because there is presently no reliable mechanism for floating an above-water system away from a measurement platform (which is easily and effectively accomplished for an in-water system), so all above-water measurements are made in close proximity to a large structure.

Despite any limitations, the above-water approach for vicarious calibration remains attractive for a number of reasons:

1. The data can presumably be collected more rapidly, and from a vessel underway;

2. The frequently turbid and strongly absorbing waters in shallow Case-2 environments impose severe limitations on in-water measurements, because of the instrument self-shading effect and the difficulty of resolving optically thin layers, particularly those close to the surface; and

3. When collecting an autonomous time series of data, the biofouling of in-air sensors is negligible in comparison to in-water sensors.

It is important to remember that above-water systems cannot be deployed in arbitrary locations, because a stable and accessible mounting location is needed to ensure the required precision for pointing the sensors with respect to the sun, the sea surface, and the sky. Note that the accessibility requirement becomes less important for a robotic system, because only limited visits associated with maintaining the equipment are required; there is no need for an operator to satisfy the pointing requirements, because this is provided automatically.

Recent studies have carefully intercompared both methodological approaches (Hooker et al. 2002a and Hooker and Morel 2003) and provided recommendations for improving above-water techniques. Many of the latter have either been incorporated into the Q01 and Q02 methods used here (e.g., using an aggressive glint filter, calculating and using a more precise surface reflectance that is wind-speed dependent, and correcting for bidirectional effects) or are part of the objectives associated with this study (e.g., quantifying and avoiding the effects of platform perturbations).

5.2 FAR-FIELD EFFECTS

The analytical results are organized by separating the data into near- and far-field categories. The former correspond to data for which $x < 13\,\mathrm{m}$ and the latter to data

for which $x \geq 13$ m (remembering that x is the perpendicular distance of the surface spot viewed by the sea-viewing sensor away from the tower). These *a priori* classification thresholds are based primarily on the Hooker and Morel (2003) study of ship perturbations on above-water radiometry, which proposed a general rule that platform perturbations (on a ship with a large superstructure) are avoidable if the sea-viewing sensor views a spot on the ocean that is approximately as far away as the platform is high.

The central variable for ocean color investigations, particularly calibration and validation activities associated with remote sensors like SeaWiFS, is the water-leaving radiance, so the distribution of this variable as a function of x is a natural starting point for investigating tower-perturbation effects. Figure 12 presents $\hat{L}_W^{Q01}(\lambda)$ for three far-field experiments from the first tower-perturbation campaign, which show significant gradients as a function of x. Not all the gradients in Fig. 12 are in keeping with the expected effects of platform reflections, which should produce an increase in L_W as x decreases.
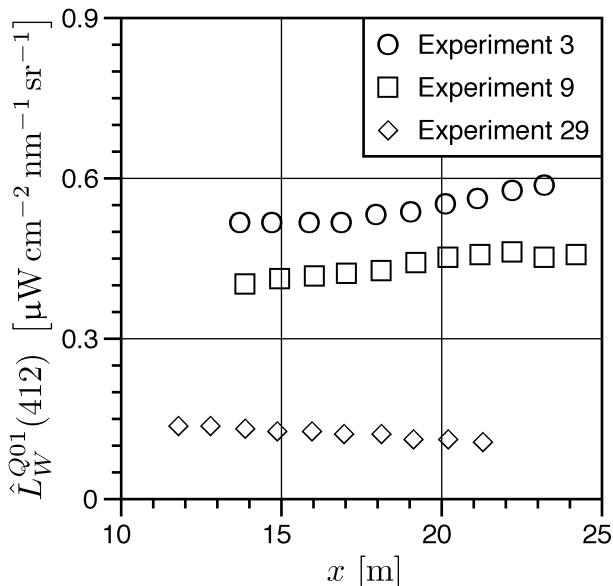
Fig. 12. A plot of the $\hat{L}_W^{Q01}(412)$ values as a function of x for three experiments in the far field ($x \geq 12$ m) of the tower.

The difficulty with using the water-leaving radiance as the primary diagnostic variable is it strongly depends on the time-dependent solar illumination. The HDS positions in experiments 3, 9, and 29 were sequenced in the same fashion from $1, 2, \ldots, 10$, so time in Fig. 12 progresses from left to right in each experiment. The gradients in Fig. 12 correspond directly to the solar evolution: experiments 3 and 9 were executed early in the morning (as the solar irradiance was increasing), and the experiment 29 data were collected in the afternoon (as the solar irradiance was decreasing).

Although an analytical approach based on the remote-sensing reflectance (5) would cancel out, in a simplified way, variations arising from changing solar illumination, a more useful parameter for perturbation studies was proposed by Hooker and Morel (2003) based on the principles involved in the glint corrections used with above-water methods.

The Morel (1980) glint correction method, hereafter referred to as M80, is based on the assumption that the sea surface is essentially *black* in the near-infrared region, λ_r. Consequently, the above-water radiance measured at λ_r is entirely due to surface reflection (principally from sky radiation once the sensor is pointed at least 90° away from the sun), and this estimate is extended over the whole spectrum by using the spectral dependence of the incident sky radiance, $L_i(\lambda)$. The estimated sky glint is subtracted from the total signal to recover $\hat{L}_W(\lambda)$, according to

$$\hat{L}_W^{M80}(\lambda, \vartheta) = L_T(\lambda, \vartheta) - L_i(\lambda, \vartheta') \left[\frac{L_T(\lambda_r, \vartheta)}{L_i(\lambda_r, \vartheta')} \right], \quad (26)$$

where again, the pointing angle with respect to the sun, ϕ', has been omitted for brevity. It is important to note that in turbid Case-2 waters, the $L_W(\lambda_r) = 0$ assumption often fails and this method is not universally applicable [see Hooker et al. (2002a) for a case example].

A comparison of the output of the M80 and S95 correction methods allows the detection of any platform contamination in the L_T signal. This is because the M80 method is sensitive to, and thus is able to identify, a platform perturbation, whereas the S95 method, based on a theoretical value of the reflectance factor, will just ignore it. The presence of a platform perturbation can be detected with the ratio

$$r(865) = \frac{L_T(865)/L_i(865)}{\rho}, \quad (27)$$

where the numerator comes from M80 (26) and the denominator from S95 (20). Under *natural* circumstances (i.e., in the absence of platform perturbations) and in Case-1 water conditions, $\rho = L_T(865)/L_i(865)$ (within the accepted variance and provided that ρ is given a correct value), and $r(865) = 1$. Any other reflected radiation added to the sky-reflected radiation leads to an increase in $L_T(865)$, and $r(865) > 1$.

The most important aspects of $r(865)$ as an analytical variable are as follows:

1. It intrinsically includes the effects of changing solar illumination, because the sea-viewing observations are normalized by the sky radiance; and

2. It is a severity index, in the sense that the stronger the artificial increase in $L_T(865)$, the larger the increase in $r(865)$, and the magnitude of the departure from unity is an estimate of the severity of the perturbation.

In Case-2 water conditions, or if the water type is close to the threshold of Case-1 and Case-2 conditions, $r(865)$ is not expected to be unity, so the last point requires some qualification: over the course of one of the tower-perturbation experiments (about 45 min on average), and in the absence of artificial reflections, $r(x, 865)$ is expected to remain essentially constant.

Departures from constancy as a function of x are expected to be an indicator of the presence of platform perturbations. Figure 13 presents $r(865)$ as a function of x for the three far-field experiments shown in Fig. 12. For all three experiments, $r(865) \approx 1$ and is nearly constant as a function of x, which indicates no tower-perturbation effects in the (above-water) water-leaving radiances.
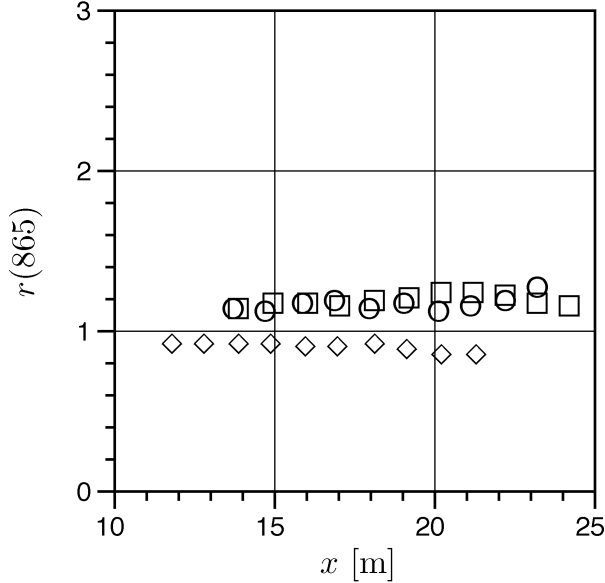
Fig. 13. A plot of $r(865)$ as a function of x for the three far-field experiments shown in Fig. 12 (using the same symbols for each experiment).

The constancy of $r(x, 865)$ can be quantified by selecting one of the farthest observations from the tower, at x', as a reference point. The RPD of the other observations within the experiment with respect to the reference point are calculated as

$$\psi_{x'}(x) = 100 \frac{r(x, 865) - r(x', 865)}{r(x', 865)}, \qquad (28)$$

where $\psi_{x'}(x)$ is the RPD value at x. Average properties cannot always be estimated accurately with RPD values, because the averaging process results in some numeric cancellation. To overcome this problem, (28) is reformulated as

$$|\psi|_{x'}(x) = 100 \frac{|r(x, 865) - r(x', 865)|}{r(x', 865)}, \qquad (29)$$

where $|\psi|$ is the absolute percent difference (APD).

Figure 14 presents the $\psi_{x'}(x)$ values for the three experiments shown in Figs. 12 and 13. The data are evenly dispersed around the $\psi_{x'} = 0$ line, which indicates there is no residual bias or trend in the data (a least-squares regression of the data has a slope of 0.05%). Given the absence of any bias or significant trend in the Fig. 14 data, the level of constancy of the far-field observations over the course of an experiment can be used to provide an estimate of the environmental variability (because this is the primary external factor influencing the variability in the data).
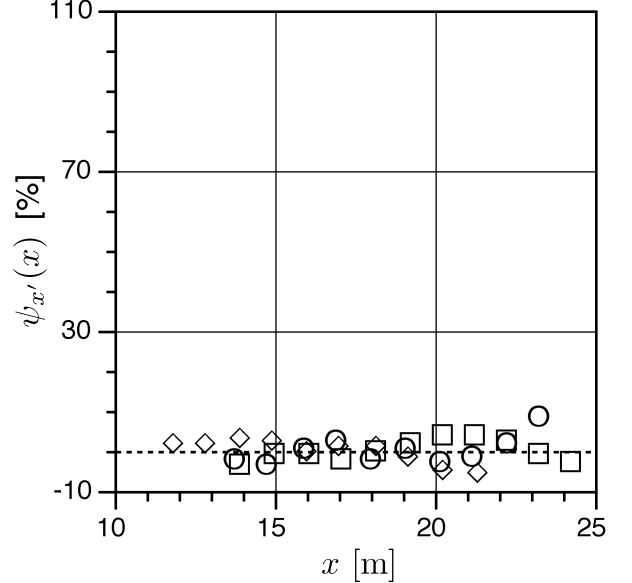
Fig. 14. A plot of $\psi_{x'}$ as a function of x for the three far-field experiments shown in Fig. 12 (using the same symbols for each experiment). The dashed line corresponds to the reference point, i.e., $\psi_{x'}(x') = 0$.

Although the above-water data processor removes the high frequency effects of glint, it does not remove environmental effects arising from surface gravity waves or the natural evolution in water properties (caused principally by advective processes for these experiments). The average APD value for the Fig. 14 data is about 2.4%, and this level of variability is in keeping with previous estimates (Hooker et al. 2002a) of the influence of environmental variability on above-water observations during long-duration experiments (which was estimated at approximately 1–3%). The environmental variability level provides a baseline variance for evaluating the presence of tower-perturbation effects in the sense that changes in $\psi_{x'}$ above this level can be attributed to artificial processes.

The far-field data confirm uncontaminated above-water observations can be collected in the vicinity of a large structure as long as the surface spot is as far away from the platform as it is high (in this case about 13 m). Although only three experiments were considered, they were all from different days, and two (experiments 3 and 9) were within similar times of the day, which means they were conducted

with similar solar geometries, and these two experiments showed very similar results.

5.3 NEAR-FIELD EFFECTS

The primary interest in executing a tower-perturbation study was to determine the spatial scale and characteristics of platform perturbations in above-water observations. The basic experiments for collecting these data were planned with the objective that the measurements start or end within the far-field environment, *a priori* set to 13 m, as often as possible (Appendices B and C). The reason for this was to ensure a suitable (unperturbed) reference point within each experiment. This sampling objective was not always applicable, however, because a variety of near-field experiments had other objectives that did not require a far-field observation.

A plot of $r(x, 865)$ for three near-field experiments from the first tower-perturbation campaign is shown in Fig. 15. As the radiometers are pointed more and more towards the tower (by varying the HDS position and the viewing angle with respect to the sun), that is as x decreases, $r(865)$ dramatically increases. The near-field $r(865)$ values are as high as 2–3 when x is about 3 m or less, which is substantially above any fluctuations that could be attributed to natural environmental variability (in the absence of floating debris). These large ratios indicate the radiation reflected by the surface and seen by the sensor is largely dominated by that originating from the tower. Furthermore, the results show the spatial extent of the tower perturbation is nonetheless about the same, approximately 11 m, which is close to the nominal height of the tower.
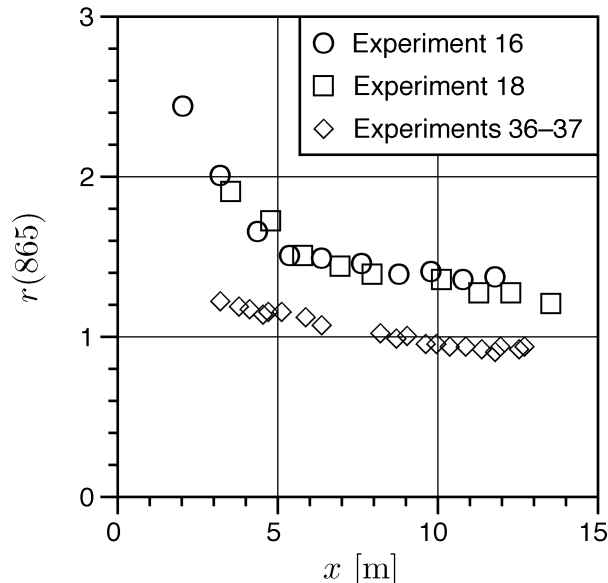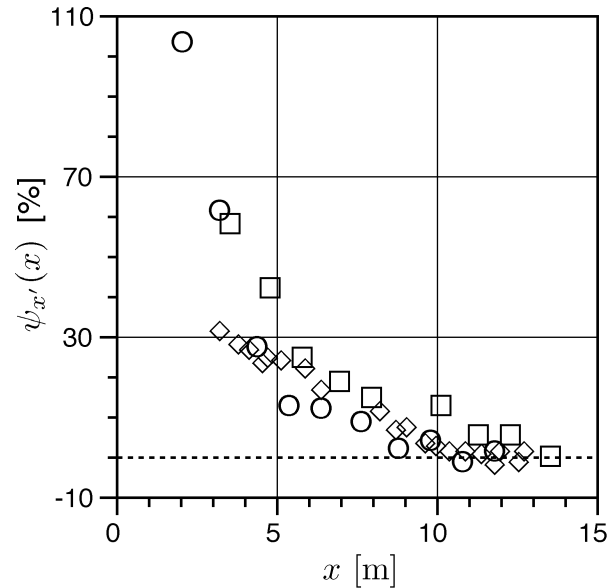

Fig. 15. A plot of $r(865)$ as a function of x for three near-field experiments.

The different amplitudes of the tower-perturbation effect during clear-sky conditions is a function of the sun

geometry. Experiments 16 and 18 were executed in the later afternoon and nearly overlie, whereas the data from experiments 36–37 were collected close to solar noon (Table B1). The larger solar zenith angles of the experiment 16 and 18 data produce larger reflections off the platform superstructure, and the lower zenith angles produce less.

The importance of the solar geometry, and the aspects of the spatial characteristics, are quantified more clearly by considering the RPD results for the near-field experiments, which are presented in Fig. 16. These data confirm the spatial extent of tower perturbations are similar for the two different solar geometries, but the amplitudes are not. The low zenith angle data (experiments 36–37) do not have as significant an amplitude as the high zenith angle data (experiments 16 and 18).

Fig. 16. A plot of $\psi_{x'}$ as a function of x for the three near-field experiments shown in Fig. 15.

5.4 ENVIRONMENTAL EFFECTS

One of the attractions of above-water measurements is the possibility of collecting data autonomously with minimal fouling of the sensors. One of the difficulties with automated systems is the absence of an observer to establish whether or not the environmental conditions are acceptable for data collection. Above-water measurements require the exclusion of floating material within the FOV of the water-viewing sensor and clouds within the FOV of the sky-viewing sensor. An observer can ensure these requirements are properly enforced, but it is more difficult to deal with automatically.

A preliminary inquiry into the effects of floating debris (grass and foam) is presented in Fig. 17. The data are from experiment 19 during the second tower-perturbation campaign, and are restricted to those observations when the HDS position was fixed. The objective here was not to collect *bad* data, but to further demonstrate the capabilities

of the $r(865)$ variable as a quality control parameter and to establish the range in differences between $r(865)$ values for uncontaminated and naturally-contaminated observations. The RPD values were calculated using the average of the uncontaminated (normal) $r(865)$ values as a reference (the dashed line).
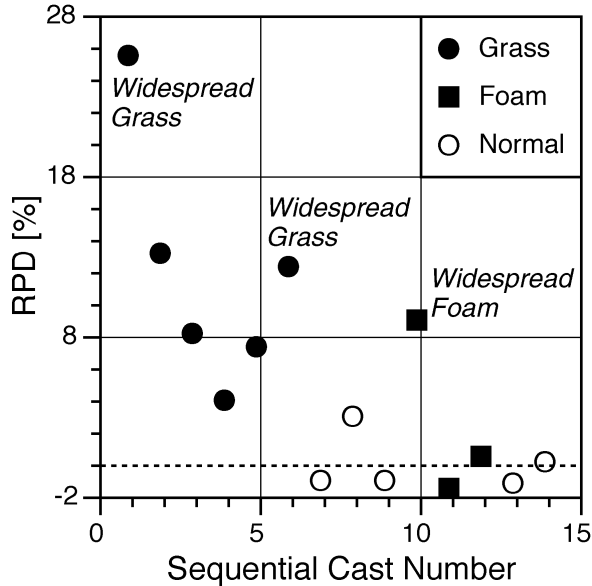
Fig. 17. A plot of the effect of floating grass and foam on above-water measurements measured during experiment 19. Casts when the grass or foam were spatially extensive are labeled "widespread."

The Fig. 17 data show natural contaminants can increase the $r(865)$ values by approximately 5–25%. It is important to remember the above-water processor selects the darkest (lowest) 5% of the L_T observations, so these results are optimized in the sense that the negative effects of the floating debris were minimized. The increases in $r(865)$ are, therefore, not the maximum that might be observed—the maximum will depend on the spatial and temporal extent of the surface contaminant within the data collection interval (in this case, the latter was 3 min). It is significant to note that there are two instances where the influence of foam on the surface was indistinguishable from the uncontaminated data, which means the standard (darkest) 5% filter can do a good job of eliminating the negative effects of floating debris in some cases.

5.5 SUMMARY

In keeping with ship perturbation experimental studies (Hooker and Morel 2003), the preliminary analysis of the tower perturbation experiments shows two results:

1. There is a similar contamination of above-water radiometric measurements due to platform reflections, and

2. Avoidance of the contamination requires the sea-viewing radiometer to view a surface spot that is approximately as far away as the tower is high.

In the simplest sense, the latter places a practical limitation on pointing the above-water sensors with respect to the platform, because the sea-viewing sensor is oriented at an angle of 40° (or 45°) with respect to nadir. Consequently, the only way to respect the distance requirement is to align the sensors within a restricted angular range perpendicular to the platform edge. The tower perturbations and, thus, the pointing requirements for the above-water sensors, depend on the geometry between the sun and the platform which is a function of the time of the day. This suggests there should be more than one mounting location for the sensors with respect to the movement of the sun which will permit uncontaminated measurements within a more extensive angular range and, therefore, during a more extensive part of the day.

S. Hooker, G. Zibordi, J-F. Berthon, D. D'Alimonte, D. van der Linde, and J. Brown

Appendices

A. Tower-Perturbation Science Team
B. The SeaBOARR-01 microSAS Deployment Log
C. The SeaBOARR-02 microSAS Deployment Log

Appendix A

Tower-Perturbation Science Team

The tower-perturbation science team members are presented alphabetically.

Jean-François Berthon
ULCO/*Maison de la Recherche en Environnement Naturel*
32 Avenue Foch
F-62930 Wimereux
FRANCE
Voice: 33–3–21–996–420
Fax: 33–3–21–996–401
Net: `berthon@mren2.univ-littoral.fr`

James Brown
MPO/RSMAS/Univ. of Miami
4600 Rickenbacker Cswy
Miami, Florida 33149
Voice: 305–361–4770
Fax: 301–361–4622
Net: `jim.brown@miami.edu`

Davide D'Alimonte
JRC/IES/IMW T.P. 272
I–21020 Ispra (VA)
ITALY
Voice: 39–0–332–785–727
Fax: 39–0–332–789–034
Net: `davide.d'alimonte@jrc.it`

Stanford Hooker
NASA/GSFC/Code 970.2
Bldg. 28, Room W126
Greenbelt, Maryland 20771
Voice: 301–286–9503
Fax: 301–286–0268
Net: `stan@ardbeg.gsfc.nasa.gov`

Dirk van der Linde
JRC/IES/IMW T.P. 272
I–21020 Ispra (VA)
ITALY
Voice: 39–0–332–785–362
Fax: 39–0–332–789–034
Net: `dirk.vanderlinde@jrc.it`

Giuseppe Zibordi
JRC/IES/IMW T.P. 272
I–21020 Ispra (VA)
ITALY
Voice: 39–0–332–785–902
Fax: 39–0–332–789–034
Net: `giuseppe.zibordi@jrc.it`

Appendix B

The SeaBOARR-01 microSAS Deployment Log

The microSAS experiment log for the first tower-perturbation campaign (SeaBOARR-01) is presented in Table B1.

Appendix C

The SeaBOARR-02 microSAS Deployment Log

The microSAS experiment log for the second tower-perturbation campaign (SeaBOARR-02) is presented in Table C1.

Glossary

AAOT	*Acqua Alta* Oceanographic Tower
AOPs	Apparent Optical Properties
APD	Absolute Percent Difference
ASCII	American Standard Code for Information Interchange
CDOM	Colored Dissolved Organic Matter
CNR	*Consiglio Nazionale delle Ricerche* (the Italian National Research Council).
CoASTS	Coastal Atmosphere and Sea Time Series
CTD	Conductivity, Temperature, and Depth
DAD	Diode Array Detector
DCP	Data Collection Platform
DIN	*Deutsche Industrie-Normen* (German industry standards).
FAFOV	Full-Angle FOV
FOV	Field of View
GF/F	Not an acronym, but a specific type of glass fiber filter manufactured by Whatman, Inc. (Clifton, New Jersey).
GMT	Greenwich Mean Time
GSFC	Goddard Space Flight Center
HDS	Horizontal Deployment System
HOBI	Hydro-Optics, Biology, and Instrumentation (Laboratories)
HPLC	High Performance Liquid Chromatography
IES	Institute for Environment Sustainability
IOCCG	International Ocean Color Coordinating Group
IOPs	Inherent Optical Properties
ISDGM	*Istituto per lo Studio della Dinamica delle Grandi Masse* (the Italian Institute for the Study of Large Masses).
JGOFS	Joint Global Ocean Flux Study
JRC	Joint Research Centre
LoCNESS	Low-Cost NASA Environmental Sampling System
METEOSAT	Meteorological Satellite
microNESS	micro NASA Environmental Sampling System
microSAS	micro Surface Acquisition System
miniNESS	miniature NASA Environmental Sampling System

Table B1. A summary of the microSAS experiments executed in the first tower perturbation campaign (SeaBOARR-01) showing the casts involved for each experiment, the Greenwich Mean Time (GMT) periods for the sampling during each sequential day of the year (SDY), the range in HDS positions, and the corresponding range in distance away from the tower, x.

Exp.	Casts	SDY	Time	Pos.	x [m]	Exp.	Casts	SDY	Time	Pos.	x [m]
1	1– 10	170	1148–1229	1–10	6.9 → 13.8	22	213–221	175	1010–1119	1	10.4 → 14.1
2	11– 20	170	1230–1310	1–10	4.3 → 10.6	23	222–230	175	1131–1231	1	4.1 → 9.3
3	21– 30	171	0852–0946	1–10	13.8 → 23.3	24	231–240	175	1246–1326	1–10	2.9 → 9.3
4	31– 40	171	1001–1047	1–10	14.3 → 22.2	25	241–250	175	1351–1423	1–10	−0.8 → 7.0
5	41– 50	171	1053–1144	1–10	12.7 → 17.8	26	251–260	175	1425–1446	1–10	−2.0 → 6.1
6	51– 60	171	1146–1231	1–10	8.3 → 13.3	27	261–270	175	1507–1550	1–10	6.1 → 20.2
7	61– 70	171	1331–1422	1–10	6.5 → 17.7	28	271–280	175	1553–1622	1–10	11.2 → 20.9
8	71– 80	172	1117–1202	1–10	10.7 → 16.1	29	281–290	175	1623–1642	1–10	11.9 → 21.5
9	81– 91	173	0904–0954	1–11	14.0 → 24.3	30	291–300	176	1002–1050	1–10	14.3 → 21.9
10	92–101	173	0957–1042	1–10	14.3 → 22.3	31	301–310	176	1105–1149	1–10	11.4 → 17.3
11	102–111	173	1049–1137	1–10	12.8 → 18.3	32	311–322	176	1204–1259	1	2.2 → 6.4
12	112–121	173	1200–1245	1–10	6.9 → 12.3	33	323–330	176	1300–1317	1	0.8 → 2.0
13	122–131	173	1247–1308	1–10	2.9 → 10.8	34	331–348	176	1456–1716	1,10	9.6 → 22.0
14	132–141	173	1434–1451	1–10	9.2 → 18.6	35	349–357	177	0945–1029	1–10	14.3 → 21.7
15	142–151	173	1455–1515	1–10	1.4 → 11.2	36	358–371	177	1031–1140	1	8.8 → 22.5
16	152–161	173	1518–1536	1–10	2.2 → 11.9	37	372–380	177	1144–1240	1	3.3 → 8.3
17	162–171	173	1540–1558	1–10	3.1 → 12.7	38	381–390	177	1259–1352	1	−1.2 → 1.6
18	172–181	173	1600–1622	1–10	3.7 → 13.7	39	391–401	177	1353–1440	1	−3.3 → −1.4
19	†183–192	175	0811–0858	1–10	14.0 → 22.1	40	402–421	177	1459–1704	1,10	−5.9 → 5.4
20	193–202	175	0900–0933	1–10	13.1 → 21.0	41	422–433	178	0859–1059	1–10	13.8 → 21.4
21	203–212	175	0944–1002	1–10	11.2 → 19.4	42	434–435	178	1108–1122	1	10.7 → 11.5

† Cast 182 was a single cast (0920–0923) on SDY 174 ($x = 12.5$ m).

Table C1. A summary of the microSAS experiments executed in the second tower perturbation campaign (SeaBOARR-02) showing the casts involved for each experiment, the GMT periods for the sampling during each SDY, the range in HDS positions, and the corresponding range in distance away from the tower, x.

Exp.	Casts	SDY	Time	Pos.	x [m]	Exp.	Casts	SDY	Time	Pos.	x [m]
1	1– 10	170	0759–0858	1–10	12.5 → 22.7	16	147–159	173	0929–1031	3	2.2 → 11.9
2	11– 16	170	0912–0941	1– 6	14.1 → 19.3	17	160–173	173	1042–1158	3	−0.8 → 14.3
3	17– 26	170	1051–1155	1–10	5.6 → 9.3	18	174–178	173	1546–1627	1– 5	3.1 → 7.3
4	27– 36	170	1211–1251	1–10	6.2 → 11.9	19	179–196	174	0635–0808	1– 9	10.3 → 20.4
5	37– 46	170	1258–1351	1–10	4.3 → 15.9	20	197–206	174	0833–0921	3	13.0 → 16.0
6	47– 56	170	1422–1503	1–10	1.2 → 8.5	21	207–216	174	0925–1010	1	11.2 → 19.4
7	57– 66	171	0826–0904	5	17.0 → 17.7	22	217–224	174	1012–1046	1	13.2 → 14.2
8	67– 76	171	0911–0955	5	18.0 → 18.3	23	225–234	174	1105–1224	3	9.1 → 13.9
9	77– 86	171	1042–1200	1–10	−1.4 → 16.8	24	235–244	174	1228–1404	5	4.6 → 10.4
10	87– 96	171	1215–1310	1–10	1.4 → 14.2	25	245–254	174	1412–1457	1–10	2.4 → 8.5
11	97–107	171	1338–1433	1–10	0.6 → 9.8	26	255–262	174	1503–1545	1– 8	1.6 → 8.7
12	108–119	172	1049–1203	5	2.3 → 17.0	27	263–281	175	0656–0830	1–10	10.6 → 20.7
13	120–129	172	1221–1317	1–10	1.4 → 14.4	28	282–292	175	0941–1041	1– 3	14.3 → 16.3
14	130–136	172	1337–1409	1–10	−0.5 → 8.7	29	293–302	175	1056–1137	1– 3	10.3 → 13.8
15	137–146	173	0811–0911	3	14.5 → 15.9	30	303–314	175	1205–1325	5	4.3 → 9.8

MREN	*Maison de la Recherche en Environnement Naturel*		S/N	Serial Number
NASA	National Aeronautics and Space Administration		SAI	Space Applications Institute
			SDY	Sequential Day of the Year
OCI	Ocean Color Irradiance		SeaBOARR	SeaWiFS Bio-Optical Algorithm Round-Robin
OCR	Ocean Color Radiance		SeaBOARR-98	The First SeaBOARR (July 1998)
			SeaBOARR-99	The Second SeaBOARR (May–June 1999)
RPD	Relative Percent Difference		SeaBOARR-00	The Third SeaBOARR (April–May 2000)
RSMAS	Rosenstiel School for Marine and Atmospheric Sciences (University of Miami)		SeaBOARR-01	The Fourth SeaBOARR (June 2001)
			SeaBOARR-02	The Fifth SeaBOARR (June 2002)
			SeaPRISM	SeaWiFS Photometer Revision for Incident

Surface Measurements

SeaSHADE The SeaWiFS shadow band attachment system.

SeaWiFS Sea-viewing Wide Field-of-view Sensor

SIAP *Societa Italiana Apparecchi di Precisione*

SUnSAS SeaWiFS Underway Surface Acquisition System

TSM Total Suspended Matter

ULCO *Université du Littoral Côte d'Opale*

WETLabs Western Environmental Technology Laboratories

WiSPER Wire-Stabilized Profiling Environmental Radiometer

WMO World Meteorological Organization

Symbols

$a(z, \lambda)$ The absorption coefficient.

$a_{dp}(z_d, \lambda)$ The absorption coefficient of nonpigmented (detritus) particles.

$a_p(\lambda)$ The total absorption coefficient.

$a_{ph}(z_d, \lambda)$ The absorption coefficient of pigmented particles (phytoplankton).

$\hat{a}_{t-w}(z, \lambda)$ The calibrated absorption coefficient.

$\hat{a}_{t-w}^{ST}(z, \lambda)$ The salinity- and temperature-corrected calibrated absorption coefficient.

$\breve{a}_{t-w}^{ST}(z, \lambda_0)$ The salinity- and temperature-corrected calibrated absorption coefficient adjusted for a variable percentage of the scattering coefficient.

$a_w(\lambda)$ The absorption coefficient of pure water.

$a_{ys}(z_d, \lambda)$ The absorption coefficient of colored dissolved organic matter (yellow substance).

$A_{\text{sus}}(\lambda)$ The equivalent particle suspension absorbance obtained from the transmission and reflection method proposed by Tassan and Ferrari (1995).

$A_{ys}(\lambda)$ The measured absorbance resulting from the difference between the sample absorbance and the reference absorbance.

$b_b(z, \lambda)$ The backscattering coefficient.

$c(z, \lambda)$ The beam attenuation coefficient.

$\hat{c}_{t-w}(z, \lambda)$ The calibrated beam attenuation coefficient.

$\hat{c}_{t-w}^{ST}(z, \lambda)$ The salinity- and temperature-corrected calibrated beam attenuation coefficient.

$c_w(\lambda)$ The beam attenuation coefficient for pure water.

C_a The chlorophyll a concentration.

C_{pig} The concentrations of phytoplankton pigments.

C_{TSM} The concentration of total suspended matter.

D D The sun–Earth distance correction factor.

D_i The distance between the instrument mounting point and the nearest support frame.

$E(\lambda)$ The direct sun irradiance.

$E_0(\lambda)$ The extra-atmospheric irradiance.

$E_b(0^+, \lambda)$ The perturbation to the diffuse irradiance field, caused by the band on a shadow band radiometer.

$E_d(0^+, \lambda)$ The total solar irradiance (the direct plus the diffuse components).

$E_d(z, \lambda)$ The downward irradiance.

$E_i(0^+, \lambda)$ The diffuse solar irradiance.

$E_m(0^+, \lambda)$ The measured (minimum) irradiance when the sun is occulted.

$E_u(z, \lambda)$ The upward irradiance.

f A function relating the irradiance reflectance to the IOPs.

f_0 The f function evaluated at a zero sun zenith.

$F_0(\lambda)$ The extraterrestrial solar flux.

F_a The filter clearance area.

F_t The flexion.

$K_L(\lambda)$ The diffuse attenuation coefficient associated with the upwelled radiance.

L_c The cuvette path length.

L_D The maximum load.

$L_i(\lambda)$ The sky radiance.

$L_T(\lambda)$ The total radiance (above the sea surface).

$L_u(z, \lambda)$ The upwelled radiance.

$L_W(\lambda)$ The water-leaving radiance.

$\tilde{L}_W(\lambda)$ The water-leaving radiance derived from an in-water measurement.

$\hat{L}_W(\lambda)$ The water-leaving radiance derived from an above-water measurement.

$\hat{L}_W^{M80}(\lambda)$ The water-leaving radiance determined using the M80 above-water method.

$\hat{L}_W^{Q01}(\lambda)$ The water-leaving radiance determined using the Q01 above-water method.

$\hat{L}_W^{S95}(\lambda)$ The water-leaving radiance determined using the S95 above-water method.

m The air mass.

$M80$ Denotes the M80 above-water method.

$n(\lambda)$ The refractive index of seawater.

$Q(\lambda)$ The bidirectional Q function.

$Q_0(\lambda)$ The Q function evaluated at nadir and a zero sun zenith.

$Q_n(\lambda)$ The Q function at nadir.

$Q01$ Denotes the Q01 above-water method.

$Q02$ Denotes the Q02 above-water method.

$r(865)$ The near-infrared radiance ratio divided by the theoretical surface reflectance.

$r_d(\lambda)$ The diffuse-to-direct irradiance ratio.

$R(\lambda)$ The irradiance reflectance.

$\Re$ The effects of reflection and refraction.

$\Re_0$ The $\Re$ function evaluated at nadir.

$R_{\text{rs}}(\lambda)$ The remote sensing reflectance.

$S95$ Denotes the S95 above-water method.

$S_s(z)$ Seawater salinity.

ST Denotes the salinity and temperature correction.

t_0 The time corresponding to the $E_m(0^+, \lambda)$ measurement.

$T_0(\lambda)$ The (upward) radiance transmittance through the air–sea interface.

$T_s(z)$ Seawater temperature.

V_w The volume of filtered water.

$\bar{w}_b$ A correction term to account for changes in the weight of the filter sample.

W Wind speed.

W_f The filter weight.

W_s The weight of the sample filter.

x The perpendicular distance of the surface spot viewed by the sea-viewing sensor away from the tower.

x' A reference point (far from the tower).

z The vertical coordinate, depth.

z_d A discrete depth.

ΔL A contamination radiance.

Δt An experimentally-determined time increment.

θ The solar zenith angle.

θ' The above-water viewing angle refracted by the air–sea interface.

ϑ The nadir angle for sea-viewing measurements.

ϑ' The zenith angle equivalent to the ϑ nadir angle ($\vartheta' = 180 - \vartheta$).

λ Wavelength.

λ_0 A reference wavelength.

λ_4 Used to indicate a four-channel sensor.

λ_7 Used to indicate a seven-channel sensor.

λ_8 Used to indicate an eight-channel sensor.

λ_i An individual channel number.

λ_r A wavelength in the near-infrared portion of the spectrum.

$\rho(\lambda)$ The (Fresnel) surface reflectance.

τ The atmospheric optical thickness.

$\tau_a(\lambda)$ The aerosol optical thickness.

$\tau_o(\lambda)$ The ozone optical thickness.

$\tau_R(\lambda)$ The Rayleigh optical thickness.

ϕ The solar azimuth angle.

ϕ' The azimuthal orientation of a sensor (usually with respect to the sun).

φ The vertical (two-axis) tilt.

ψ The relative percent difference.

$|\psi|$ The absolute percent difference.

$\psi_{x'}$ The relative percent difference based on a reference measurement at x'.

$|\psi|_{x'}$ The absolute percent difference based on a reference measurement at x'.

Ω_{FOV} The solid angle (field of view) of the detector.

References

Aiken, J., D.G. Cummings, S.W. Gibb, N.W. Rees, R. Woodd-Walker, E.M.S. Woodward, J. Woolfenden, S.B. Hooker, J-F. Berthon, C.D. Dempsey, D.J. Suggett, P. Wood, C. Donlon, N. González-Benítez, I. Huskin, M. Quevedo, R. Barciela-Fernandez, C. de Vargas, and C. McKee, 1998: AMT-5 Cruise Report. *NASA Tech. Memo. 1998–206892, Vol. 2,* S.B. Hooker and E.R. Firestone, Eds., NASA Goddard Space Flight Center, Greenbelt, Maryland, 113 pp.

Austin, R.W., 1974: "The Remote Sensing of Spectral Radiance from Below the Ocean Surface." In: *Optical Aspects of Oceanography,* N.G. Jerlov and E.S. Nielsen, Eds., Academic Press, London, 317–344.

Berthon, J-F., G. Zibordi, J.P. Doyle, S. Grossi, D. van der Linde, and C. Targa, 2002: Coastal Atmosphere and Sea Time Series (CoASTS), Part 2: Data Analysis. *NASA Tech. Memo. 2002–206892, Vol. 20,* S.B. Hooker and E.R. Firestone, Eds., NASA Goddard Space Flight Center, Greenbelt, Maryland, 25 pp.

Bonzagni, M., U. Amato, R. Rizzi, and R. Guzzi, 1989: Evaluation of the shadowband effect on a 2π spectroradiometer. *Appl. Opt.,* **28,** 2,199–2,201.

Carder, K.L., and R.G. Steward, 1985: A remote sensing reflectance model of a red tide dinoflagellate off West Florida. *Limnol. Oceanogr.,* **30,** 286–298.

Doyle, J.P., and G. Zibordi, 2002: Optical propagation within a 3-dimensional shadowed atmosphere–ocean field: Application to large deployment structures. *Appl. Opt.,* **41,** 4,283–4,306.

Ferrari, G.M., and S. Tassan, 1999: A method using chemical oxidation to remove light absorption by phytoplankton pigments. *J. Phycol.,* **35,** 1,090–1,098.

——, M.D. Dowell, S. Grossi, and C. Targa, 1996: Relationship between the optical properties of chromophoric dissolved organic matter and total concentration of dissolved organic carbon in the southern Baltic Sea region. *Mar. Chem.,* **55,** 299–316.

Gordon, H.R., and D.K. Clark, 1981: Clear water radiances for atmospheric correction of coastal zone color scanner imagery. *Appl. Opt.,* **20,** 4,175–4,180.

——, and K. Ding, 1992: Self-shading of in-water optical instruments, *Limnol. Oceanogr.,* **37,** 491–500.

Guzzi, R., G. Maracci, R. Rizzi, and R. Siccardi, 1985: Spectroradiometer for ground-based atmospheric measurements related to remote sensing in the visible from a satellite. *Appl. Opt.,* **24,** 2,859–2,864.

Harrison, L., J. Michalsky, and J. Berndt, 1994: Automated multifilter rotating shadow band radiometer: An instrument for optical depth and radiation measurements, *Appl. Opt.,* **33,** 5,118–5,125.

Holben, B.N., T.F. Eck, I. Slutsker, D. Tanré, J.P. Buis, A. Setzer, E. Vermote, J.A. Reagan, Y.I. Kaufman, T. Nakajima, F. Lavenu, I. Jankowiak, and A. Smirnov, 1998: AERONET—A federated instrument network and data archive for aerosol characterization. *Remote Sens. Environ.,* **66,** 1–16.

Hooker, S.B., and W.E. Esaias, 1993: An overview of the Sea-WiFS project. *Eos, Trans., Amer. Geophys. Union,* **74,** 241–246

——, G. Zibordi, G. Lazin, and S. McLean, 1999: The Sea-BOARR-98 Field Campaign. *NASA Tech. Memo. 1999–206892, Vol. 3,* S.B. Hooker and E.R. Firestone, Eds., NASA Goddard Space Flight Center, Greenbelt, Maryland, 40 pp.

——, and G. Lazin, 2000: The SeaBOARR-99 Field Campaign. *NASA Tech. Memo. 2000–206892, Vol. 8,* S.B. Hooker and E.R. Firestone, Eds., NASA Goddard Space Flight Center, 46 pp.

——, and S. Maritorena, 2000: An evaluation of oceanographic radiometers and deployment methodologies. *J. Atmos. Ocean. Technol.,* **17,** 811–830.

——, and C.R. McClain, 2000: The calibration and validation of SeaWiFS data. *Prog. Oceanogr.,* **45,** 427–465.

——, G. Zibordi, J-F. Berthon, S.W. Bailey, and C.M. Pietras, 2000a: The SeaWiFS Photometer Revision for Incident Surface Measurement (SeaPRISM) Field Commissioning. *NASA Tech. Memo. 2000–206892, Vol. 13,* S.B. Hooker and E.R. Firestone, Eds., NASA Goddard Space Flight Center, Greenbelt, Maryland, 24 pp.

——, H. Claustre, J. Ras, L. Van Heukelem, J-F. Berthon, C. Targa, D. van der Linde, R. Barlow, and H. Sessions, 2000b: The First SeaWiFS HPLC Analysis Round-Robin Experiment (SeaHARRE-1). *NASA Tech. Memo. 2000–206892, Vol. 14,* S.B. Hooker and E.R. Firestone, Eds., NASA Goddard Space Flight Center, Greenbelt, Maryland, 42 pp.

——, G. Lazin, G. Zibordi, and S. McLean, 2002a: An evaluation of above- and in-water methods for determining water-leaving radiances. *J. Atmos. Ocean. Technol.,* **19,** 486–515.

——, S. McLean, J. Sherman, M. Small, G. Lazin, G. Zibordi, and J.W. Brown, 2002b: The Seventh SeaWiFS Intercalibration Round-Robin Experiment (SIRREX-7), March 1999. *NASA Tech. Memo. 2002–206892, Vol. 17,* S.B. Hooker and E.R. Firestone, Eds., NASA Goddard Space Flight Center, Greenbelt, Maryland, 69 pp.

——, and A. Morel, 2003: Platform and environmental effects on above- and in-water determinations of water-leaving radiances. *J. Atmos. Ocean. Technol.,* **20,** 187–205.

IOCCG, 1998: Minimum Requirements for an Operational Ocean-Colour Sensor for the Open Ocean. *Reports Int. Ocean-Colour Coord. Group, Rept. No. 1,* Int. Ocean-Colour Coord. Group, Nova Scotia, Canada, 46 pp.

Joint Global Ocean Flux Study, 1994: Protocols for the Joint Global Ocean Flux Study Core Measurements. Intergovernmental Oceanographic Commission, *SCOR, Manual and Guides, UNESCO,* Paris, France, **29,** 91–96.

Lazin, G., 1998: Correction Methods for Low-Altitude Remote Sensing of Ocean Color. *M.Sc. Thesis,* Dalhousie University, Halifax, Nova Scotia, 98 pp.

Maffione, R.A., and D.R. Dana, 1997: Instruments and methods for measuring the backward-scattering coefficient of ocean waters. *Appl. Opt.,* **36,** 6,057–6,067.

McClain, C.R., W.E. Esaias, W. Barnes, B. Guenther, D. Endres, S. Hooker, G. Mitchell, and R. Barnes, 1992: Calibration and Validation Plan for SeaWiFS. *NASA Tech. Memo. 104566, Vol. 3,* S.B. Hooker and E.R. Firestone, Eds., 41 pp.

——, M.L. Cleave, G.C. Feldman, W.W. Gregg, and S.B. Hooker, 1998: Science quality SeaWiFS data for global biosphere research. *Sea Technol.,* **39,** 10–15.

Mobley, C.D., 1999: Estimation of the remote-sensing reflectance from above-surface measurements. *Appl. Opt.,* **38,** 7,442–7,455.

Morel, A., 1980: In-water and remote measurements of ocean color. *Bound.-Layer Meteorol.,* **18,** 177–201.

——, and L. Prieur, 1977: Analysis of variations in ocean color. *Limnol. Oceanogr.,* **22,** 709–722.

——, and B. Gentili, 1996: Diffuse reflectance of oceanic waters, III. Implication of bidirectionality for the remote sensing problem. *Appl. Opt.,* **35,** 4,850–4,862.

——, and J.L. Mueller, 2002: "Normalized Water-Leaving Radiance and Remote Sensing Reflectance: Bidirectional Reflectance and Other Factors." In: J.L. Mueller and G.S. Fargion, Ocean Optics Protocols for Satellite Ocean Color Sensor Validation, Revision 3, Volume 2. *NASA Tech. Memo. 2002–210004/Rev3–Vol2,* NASA Goddard Space Flight Center, Greenbelt, Maryland, 183–210.

——, D. Antoine, and B. Gentilli, 2002: Bidirectional reflectance of oceanic waters: Accounting for Raman emission and varying particle scattering phase function. *Appl. Opt.,* **41,** 6,289–6,306.

Mueller, J.L., 2000: "Overview of Measurement and Data Analysis Protocols" and "In-water radiometric profile measurements and data analysis protocols." In: G.S. Fargion and J.L. Mueller, Ocean Optics Protocols for Satellite Ocean Color Sensor Validation, Revision 2. *NASA Tech. Memo. 2000–209966,* NASA Goddard Space Flight Center, Greenbelt, Maryland, 87–97.

——, 2002: "Overview of Measurement and Data Analysis Protocols." In: J.L. Mueller and G.S. Fargion, Ocean Optics Protocols for Satellite Ocean Color Sensor Validation, Revision 3, Volume 1. *NASA Tech. Memo. 2002–210004/Rev3–Vol1,* NASA Goddard Space Flight Center, Greenbelt, Maryland, 123–137.

——, and R.W. Austin, 1992: Ocean Optics Protocols for SeaWiFS Validation. *NASA Tech. Memo. 104566, Vol. 5,* S.B. Hooker and E.R. Firestone, Eds., NASA Goddard Space Flight Center, Greenbelt, Maryland, 43 pp.

——, and ——, 1995: Ocean Optics Protocols for SeaWiFS Validation, Revision 1. *NASA Tech. Memo. 104566, Vol. 25,* S.B. Hooker, E.R. Firestone, and J.G. Acker, Eds., NASA Goddard Space Flight Center, Greenbelt, Maryland, 66 pp.

——, and A. Morel, 2002: "Fundamental Definitions, Relationships and Conventions." In: J.L. Mueller and G.S. Fargion, Ocean Optics Protocols for Satellite Ocean Color Sensor Validation, Revision 3, Volume 1. *NASA Tech. Memo. 2002–210004/Rev3–Vol1,* NASA Goddard Space Flight Center, Greenbelt, Maryland, 10–28.

——, C. Davis, R. Arnone, R. Frouin, K. Carder, Z.P. Lee, R.G. Steward, S. Hooker, C.D. Mobley, and S. McLean, 2002: "Above-Water Radiance and Remote Sensing Reflectance Measurement and Analysis Protocols." In: J.L. Mueller and G.S. Fargion, Ocean Optics Protocols for Satellite Ocean Color Sensor Validation, Revision 3, Volume 2. *NASA Tech. Memo. 2002–210004/Rev3–Vol2,* NASA Goddard Space Flight Center, Greenbelt, Maryland, 171–182.

Neckel, H., and D. Labs, 1984: The solar radiation between 3300 and 12500 Å. *Sol. Phys.,* **90,** 205–258.

Pope, R.M., and E.S. Fry, 1997: Absorption spectrum (380–700 nm) of pure water, II. Integrating cavity measurements, *Appl. Opt.,* **36,** 8,710–8,723.

Strickland, J.D.H., and T.R. Parsons, 1972: *A Practical Handbook of Sea Water Analysis.* Fish. Res. Board., Canada, 310 pp.

Tassan, S., and G.M. Ferrari, 1995: An alternative approach to absorption measurements of aquatic particles retained on filters, *Limnol. Oceanogr.,* **40,** 1,358–1,368.

van der Linde, D., 2003: The AAOT Deployment Systems: An Overview. *EUR Report 20548 EN,* Joint Research Centre, Ispra, Italy, 13 pp.

WETLabs, 2002: *AC-9 Protocol Document.* [World Wide Web page.] From URL: `http://www.wetlabs.com/Products /pub/ac9/` WETLabs, Inc., Philomath, Oregon.

World Meteorological Organization, 1983: *Guide to the Meteorological Instruments and Methods of Observation,* WMO–N.8, 517 pp.

Wright, S.W., S.W. Jeffrey, F.C. Mantoura, C.A. Llewellyn, T. Bjørnland, D. Repeta, and N. Welschmeyer, 1991: Improved HPLC method for the analysis of chlorophylls and carotenoids from marine phytoplankton. *Mar. Ecol. Prog. Ser.,* **77,** 183–196.

Zaneveld, J.R., J.C. Kitchen, and C. Moore, 1994: The scattering error coefficient of reflective absorption measurements. *SPIE, Ocean Optics XII,* **2,258,** 44–54.

Zibordi, G., S.B. Hooker, J-F. Berthon, and D. D'Alimonte. 2002a: Autonomous above-water radiance measurements from an offshore platform: A field assessment experiment. *J. Atmos. Ocean. Technol.,* **19,** 808–819.

——, J-F. Berthon, J.P. Doyle, S. Grossi, D. van der Linde, C. Targa, and L. Alberotanza, 2002b: Coastal Atmosphere and Sea Time Series (CoASTS), Part 1: A Tower-Based Long-Term Measurement Program. *NASA Tech. Memo. 2002–206892, Vol. 19,* S.B. Hooker and E.R. Firestone, Eds., NASA Goddard Space Flight Center, Greenbelt, Maryland, 29 pp.

THE SEAWIFS POSTLAUNCH
TECHNICAL REPORT SERIES

Vol. 1

Johnson, B.C., J.B. Fowler, and C.L. Cromer, 1998: The Sea-WiFS Transfer Radiometer (SXR). *NASA Tech. Memo. 1998–206892, Vol. 1,* S.B. Hooker and E.R. Firestone, Eds., NASA Goddard Space Flight Center, Greenbelt, Maryland, 58 pp.

Vol. 2

Aiken, J., D.G. Cummings, S.W. Gibb, N.W. Rees, R. Woodd-Walker, E.M.S. Woodward, J. Woolfenden, S.B. Hooker, J-F. Berthon, C.D. Dempsey, D.J. Suggett, P. Wood, C. Donlon, N. González-Benítez, I. Huskin, M. Quevedo, R. Barciela-Fernandez, C. de Vargas, and C. McKee, 1998: AMT-5 Cruise Report. *NASA Tech. Memo. 1998–206892, Vol. 2,* S.B. Hooker and E.R. Firestone, Eds., NASA Goddard Space Flight Center, Greenbelt, Maryland, 113 pp.

Vol. 3

Hooker, S.B., G. Zibordi, G. Lazin, and S. McLean, 1999: The SeaBOARR-98 Field Campaign. *NASA Tech. Memo. 1999–206892, Vol. 3,* S.B. Hooker and E.R. Firestone, Eds., NASA Goddard Space Flight Center, Greenbelt, Maryland, 40 pp.

Vol. 4

Johnson, B.C., E.A. Early, R.E. Eplee, Jr., R.A. Barnes, and R.T. Caffrey, 1999: The 1997 Prelaunch Radiometric Calibration of SeaWiFS. *NASA Tech. Memo. 1999–206892, Vol. 4,* S.B. Hooker and E.R. Firestone, Eds., NASA Goddard Space Flight Center, Greenbelt, Maryland, 51 pp.

Vol. 5

Barnes, R.A., R.E. Eplee, Jr., S.F. Biggar, K.J. Thome, E.F. Zalewski, P.N. Slater, and A.W. Holmes 1999: The Sea-WiFS Solar Radiation-Based Calibration and the Transfer-to-Orbit Experiment. *NASA Tech. Memo. 1999–206892, Vol. 5,* S.B. Hooker and E.R. Firestone, Eds., NASA Goddard Space Flight Center, 28 pp.

Vol. 6

Firestone, E.R., and S.B. Hooker, 2000: SeaWiFS Postlaunch Technical Report Series Cumulative Index: Volumes 1–5. *NASA Tech. Memo. 2000–206892, Vol. 6,* S.B. Hooker and E.R. Firestone, Eds., NASA Goddard Space Flight Center, Greenbelt, Maryland, 14 pp.

Vol. 7

Johnson, B.C., H.W. Yoon, S.S. Bruce, P-S. Shaw, A. Thompson, S.B. Hooker, R.E. Eplee, Jr., R.A. Barnes, S. Maritorena, and J.L. Mueller, 1999: The Fifth SeaWiFS Intercalibration Round-Robin Experiment (SIRREX-5), July 1996. *NASA Tech. Memo. 1999–206892, Vol. 7,* S.B. Hooker and E.R. Firestone, Eds., NASA Goddard Space Flight Center, 75 pp.

Vol. 8

Hooker, S.B., and G. Lazin, 2000: The SeaBOARR-99 Field Campaign. *NASA Tech. Memo. 2000–206892, Vol. 8,* S.B. Hooker and E.R. Firestone, Eds., NASA Goddard Space Flight Center, 46 pp.

Vol. 9

McClain, C.R., E.J. Ainsworth, R.A. Barnes, R.E. Eplee, Jr., F.S. Patt, W.D. Robinson, M. Wang, and S.W. Bailey, 2000: SeaWiFS Postlaunch Calibration and Validation Analyses, Part 1. *NASA Tech. Memo. 2000–206892, Vol. 9,* S.B. Hooker and E.R. Firestone, Eds., NASA Goddard Space Flight Center, 82 pp.

Vol. 10

McClain, C.R., R.A. Barnes, R.E. Eplee, Jr., B.A. Franz, N.C. Hsu, F.S. Patt, C.M. Pietras, W.D. Robinson, B.D. Schieber, G.M. Schmidt, M. Wang, S.W. Bailey, and P.J. Werdell, 2000: SeaWiFS Postlaunch Calibration and Validation Analyses, Part 2. *NASA Tech. Memo. 2000–206892, Vol. 10,* S.B. Hooker and E.R. Firestone, Eds., NASA Goddard Space Flight Center, 57 pp.

Vol. 11

O'Reilly, J.E., S. Maritorena, M.C. O'Brien, D.A. Siegel, D. Toole, D. Menzies, R.C. Smith, J.L. Mueller, B.G. Mitchell, M. Kahru, F.P. Chavez, P. Strutton, G.F. Cota, S.B. Hooker, C.R. McClain, K.L. Carder, F. Müller-Karger, L. Harding, A. Magnuson, D. Phinney, G.F. Moore, J. Aiken, K.R. Arrigo, R. Letelier, and M. Culver 2000: SeaWiFS Postlaunch Calibration and Validation Analyses, Part 3. *NASA Tech. Memo. 2000–206892, Vol. 11,* S.B. Hooker and E.R. Firestone, Eds., NASA Goddard Space Flight Center, 49 pp.

Vol. 12

Firestone, E.R., and S.B. Hooker, 2000: SeaWiFS Postlaunch Technical Report Series Cumulative Index: Volumes 1–11. *NASA Tech. Memo. 2000–206892, Vol. 12,* S.B. Hooker and E.R. Firestone, Eds., NASA Goddard Space Flight Center, Greenbelt, Maryland, 24 pp.

Vol. 13

Hooker, S.B., G. Zibordi, J-F. Berthon, S.W. Bailey, and C.M. Pietras, 2000: The SeaWiFS Photometer Revision for Incident Surface Measurement (SeaPRISM) Field Commissioning. *NASA Tech. Memo. 2000–206892, Vol. 13,* S.B. Hooker and E.R. Firestone, Eds., NASA Goddard Space Flight Center, Greenbelt, Maryland, 24 pp.

Vol. 14

Hooker, S.B., H. Claustre, J. Ras, L. Van Heukelem, J-F. Berthon, C. Targa, D. van der Linde, R. Barlow, and H. Sessions, 2000: The First SeaWiFS HPLC Analysis Round-Robin Experiment (SeaHARRE-1). *NASA Tech. Memo. 2000–206892, Vol. 14,* S.B. Hooker and E.R. Firestone, Eds., NASA Goddard Space Flight Center, Greenbelt, Maryland, 42 pp.

Vol. 15

Hooker, S.B., G. Zibordi, J-F. Berthon, D. D'Alimonte, S. Maritorena, S. McLean, and J. Sildam, 2001: Results of the Second SeaWiFS Data Analysis Round Robin, March 2000 (DARR-00). *NASA Tech. Memo. 2001–206892, Vol. 15,* S.B. Hooker and E.R. Firestone, Eds., NASA Goddard Space Flight Center, Greenbelt, Maryland, 71 pp.

Vol. 16

Patt, F.S., 2002: Navigation Algorithms for the SeaWiFS Mission. *NASA Tech. Memo. 2002–206892, Vol. 16,* S.B. Hooker and E.R. Firestone, Eds., NASA Goddard Space Flight Center, Greenbelt, Maryland, 17 pp.

Vol. 17

Hooker, S.B., S. McLean, J. Sherman, M. Small, G. Lazin, G. Zibordi, and J.W. Brown, 2002: The Seventh SeaWiFS Intercalibration Round-Robin Experiment (SIRREX-7), March 1999. *NASA Tech. Memo. 2002–206892, Vol. 17,* S.B. Hooker and E.R. Firestone, Eds., NASA Goddard Space Flight Center, Greenbelt, Maryland, 69 pp.

Vol. 18

Firestone, E.R., and S.B. Hooker, 2003: SeaWiFS Postlaunch Technical Report Series Cumulative Index: Volumes 1–17. *NASA Tech. Memo. 2003–206892, Vol. 18,* S.B. Hooker and E.R. Firestone, Eds., NASA Goddard Space Flight Center, Greenbelt, Maryland, 28 pp.

Vol. 19

Zibordi, G., J-F. Berthon, J.P. Doyle, S. Grossi, D. van der Linde, C. Targa, and L. Alberotanza 2002: Coastal Atmosphere and Sea Time Series (CoASTS), Part 1: A Tower-Based Long-Term Measurement Program. *NASA Tech. Memo. 2002–206892, Vol. 19,* S.B. Hooker and E.R. Firestone, Eds., NASA Goddard Space Flight Center, Greenbelt, Maryland, 29 pp.

Vol. 20

Berthon, J-F., G. Zibordi, J.P. Doyle, S. Grossi, D. van der Linde, and C. Targa, 2002: Coastal Atmosphere and Sea Time Series (CoASTS), Part 2: Data Analysis. *NASA Tech. Memo. 2002–206892, Vol. 20,* S.B. Hooker and E.R. Firestone, Eds., NASA Goddard Space Flight Center, Greenbelt, Maryland, 25 pp.

Vol. 21

Zibordi, G., D. D'Alimonte, D. van der Linde, J-F. Berthon, S.B. Hooker, J.L. Mueller, G. Lazin, and S. McLean, 2002: The Eighth SeaWiFS Intercalibration Round-Robin Experiment (SIRREX-8), September–December 2001. *NASA Tech. Memo. 2002–206892, Vol. 21,* S.B. Hooker and E.R. Firestone, Eds., NASA Goddard Space Flight Center, Greenbelt, Maryland, 39 pp.

Vol. 22

Patt, F.S., R.A. Barnes, R.E. Eplee, Jr., B.A. Franz, W.D. Robinson, G.C. Feldman, S.W. Bailey J. Gales, P.J. Werdell, M. Wang, R. Frouin, R.P. Stumpf, R.A. Arnone, R.W. Gould, Jr., P.M. Martinolich, V. Ransibrahmanakul, J.E. O'Reilly, and J.A. Yoder, 2003: Algorithm Updates for the Fourth SeaWiFS Data Reprocessing, *NASA Tech. Memo. 2003–206892, Vol. 22,* S.B. Hooker and E.R. Firestone, Eds., NASA Goddard Space Flight Center, Greenbelt, Maryland, 74 pp.

Vol. 23

Hooker, S.B., G. Zibordi, J-F. Berthon, D. D'Alimonte, D. van der Linde, and J.W. Brown, 2003: Tower-Perturbation Measurements in Above-Water Radiometry. *NASA Tech. Memo. 2003–206892, Vol. 23,* S.B. Hooker and E.R. Firestone, Eds., NASA Goddard Space Flight Center, Greenbelt, Maryland, 35 pp.

REPORT DOCUMENTATION PAGE

1. AGENCY USE ONLY *(Leave blank)*	2. REPORT DATE May 2003	3. REPORT TYPE AND DATES COVERED Technical Memorandum

4. TITLE AND SUBTITLE

SeaWiFS Postlaunch Technical Report Series
Volume 23: Tower-Perturbation Measurements in Above-Water Radiometry

5. FUNDING NUMBERS

970.2

6. AUTHORS

S.B. Hooker, G. Zibordi, J-F. Berthon, D. D'Alimonte, D. van der Linde, and J.W. Brown

Series Editors: Stanford B. Hooker and Elaine R. Firestone

7. PERFORMING ORGANIZATION NAME(S) AND ADDRESS(ES)

Laboratory for Hydrospheric Processes
Goddard Space Flight Center
Greenbelt, Maryland 20771

8. PERFORMING ORGANIZATION REPORT NUMBER

2003-01914-0

9. SPONSORING/MONITORING AGENCY NAME(S) AND ADDRESS(ES)

National Aeronautics and Space Administration
Washington, D.C. 20546–0001

10. SPONSORING/MONITORING AGENCY REPORT NUMBER

TM—2003–206892, Vol. 23

11. SUPPLEMENTARY NOTES

E.R. Firestone: Science Applications International Corporation, Beltsville, Maryland; G. Zibordi, J-F. Berthon, D. D'Alimonte, and D. van der Linde: JRC/Institute for Environment and Sustainability, Ispra, Italy; J.W. Brown: RSMAS University of Miami, Miami, Florida

12a. DISTRIBUTION/AVAILABILITY STATEMENT

12b. DISTRIBUTION CODE

13. ABSTRACT *(Maximum 200 words)*

This report documents the scientific activities which took place during June 2001 and June 2002 on the *Acqua Alta* Oceanographic Tower (AAOT) in the northern Adriatic Sea. The primary objective of these field campaigns was to quantify the effect of platform perturbations (principally reflections of sunlight onto the sea surface) on above-water measurements of water-leaving radiances. The deployment goals documented in this report were to: a) collect an extensive and simultaneous set of above- and in-water optical measurements under predominantly clear-sky conditions; b) establish the vertical properties of the water column using a variety of ancillary measurements, many of which were taken coincidently with the optical measurements; and c) determine the bulk properties of the environment using a diversity of atmospheric, biogeochemical, and meteorological techniques. A preliminary assessment of the data collected during the two field campaigns shows the perturbation in above-water radiometry caused by a large offshore structure is very similar to that caused by a large research vessel.

14. SUBJECT TERMS

SeaWiFS, Oceanography, Tower-Perturbation Measurements, Above-Water, Radiometry, In-Water, Data Processing Methods, In Situ Sampling

15. NUMBER OF PAGES

35

16. PRICE CODE

17. SECURITY CLASSIFICATION OF REPORT	18. SECURITY CLASSIFICATION OF THIS PAGE	19. SECURITY CLASSIFICATION OF ABSTRACT	20. LIMITATION OF ABSTRACT
Unclassified	Unclassified	Unclassified	Unlimited